



---

# High Gain Spatial Photon Correlations

---

THESIS

submitted in partial fulfillment of the  
requirements for the degree of

BACHELOR OF SCIENCE

in

PHYSICS

Author :	Mio Poortvliet
Student ID :	s2071827
Supervisor :	Wolfgang Löffler
2 <sup>nd</sup> corrector :	Serge Fehr

Leiden, The Netherlands, July 10, 2020



# High Gain Spatial Photon Correlations

**Mio Poortvliet**

Huygens-Kamerlingh Onnes Laboratory, Leiden University  
P.O. Box 9500, 2300 RA Leiden, The Netherlands

July 10, 2020

## **Abstract**

Spontaneous parametric down-conversion is a non-linear optical process mediated by a crystal where an incident photon is converted into two or more outgoing photons. The theory describing parametric down-conversion is studied; multi-photon correlations in a spatial basis and orbital angular momentum basis are studied theoretically and experimentally. For high intensity pump fields multiple photon pairs can be created. This is investigated experimentally and by simulation. Theory is developed to describe orbital angular momentum for multiple photon pairs and is applied to double photon pairs. Progress is made to differentiate between spontaneous and stimulated double photon pair emissions.



# Contents

<b>1</b>	<b>Introduction</b>	<b>1</b>
<b>2</b>	<b>Gaussian Beams</b>	<b>3</b>
2.1	Paraxial Wave Equation	3
2.2	Gaussian Solutions	4
2.3	Hermite-Gauss and Laguerre-Gauss modes	5
2.3.1	Hermite-Gauss	5
2.3.2	Laguerre-Gauss	5
2.4	Orbital Angular Momentum	6
<b>3</b>	<b>Non-Linear Interactions in a Crystal</b>	<b>7</b>
3.1	Linear effects	7
3.1.1	Permittivity Tensor	8
3.1.2	Index Ellipsoid	9
3.1.3	Linear Electro-Optic Effect	9
3.2	First Order Non-Linear Effects	10
3.2.1	Non-Linear Optical Susceptibility Tensor	10
3.2.2	Work	11
<b>4</b>	<b>Spontaneous Parametric Down-Conversion</b>	<b>13</b>
4.1	Classical Formulation	13
4.1.1	Equations for three fields	14
4.1.2	Energy density	16
4.2	Quantum Hamiltonian	17
4.3	Phase Matching	20
4.3.1	Periodic Poling	20
4.4	Structure of SPDC Light	21
4.4.1	Half-angle divergence of degenerate SPDC light	22

---

4.4.2	Klyshko Picture	23
4.4.3	Degenerate Collinear Bi-photon Wave Function	23
4.5	Conservation of Orbital Angular Momentum	27
4.5.1	Schmidt Decomposition and Schmidt Number	28
4.5.2	Decomposition of the Biphoton Wavefunction	28
4.5.3	Calculating the Coefficients	29
4.5.4	Explicitly Showing Conservation of OAM	30
<b>5</b>	<b>Four Photon Type-I PDC</b>	<b>31</b>
5.1	Spontaneous or Stimulated Emission?	32
5.2	Approximation of the PDC State	32
5.2.1	Momentum Basis	33
5.2.2	Orbital Angular Momentum Basis	33
5.3	Spatial PDC Field	36
<b>6</b>	<b>Experimental Setup</b>	<b>39</b>
6.1	Optics	39
6.2	SLMs	41
6.3	Coincidence counts	41
6.4	Anti-Correlation of Orbital Angular Momentum	41
<b>7</b>	<b>Results</b>	<b>43</b>
7.1	Conservation of Orbital Angular Momentum	43
7.2	Power Dependent Counts	43
7.2.1	Single Counts	44
7.2.2	Coincidence Counts	45
7.3	Numerical Experiments	46
7.3.1	Spatial Correlations	47
<b>8</b>	<b>Discussion</b>	<b>51</b>
8.1	Conservation of Orbital Angular Momentum	51
8.2	Power Dependent Counts	51
8.3	Four Photon Correlation Function	52
8.4	Reflecting on the Experiment	52
<b>A</b>	<b>Towards the Derivation of a Fourth Order Correlation Function</b>	<b>55</b>
A.1	Wick's Theorem	55
A.2	Four Detector Correlations	56
A.2.1	Single Pair Contributions	58
A.2.2	Double Pair Wave Function	62
<b>B</b>	<b>Simulation</b>	<b>65</b>

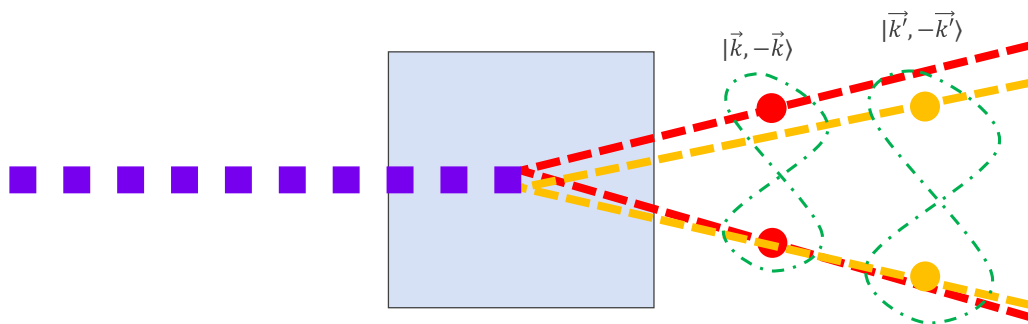
---

# Introduction

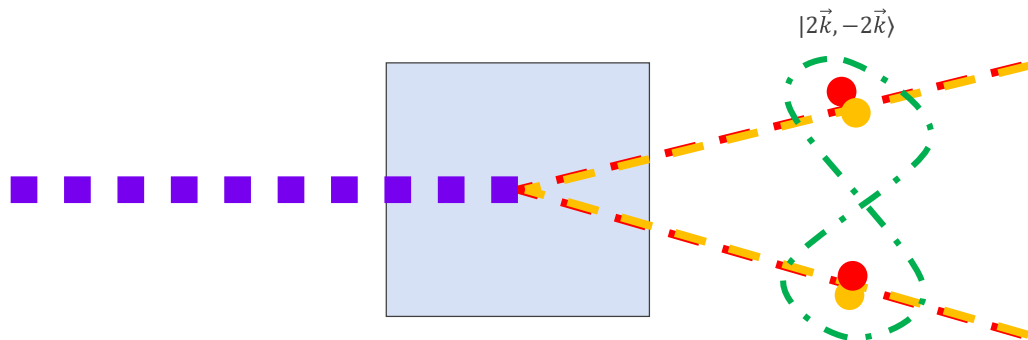
Quantum entanglement is an often misunderstood subject in popular science. This seemingly paradoxical phenomenon has been called ‘spooky action at a distance’ [1] and nowadays is misused to justify pseudo-science as ‘quantum woo’. As we understand it today, quantum entanglement arises naturally from certain phenomena. One particle can affect another at a distance, but it is not considered spooky anymore. Entangled systems are commonplace in modern physics laboratory, our experiment is no different. Quantum entanglement of more than two photons has possible applications in multi-party quantum secret sharing [2–6], optically propagating neural networks at the speed of light, high bandwidth optical data transfer [7] using existing infrastructure and more fundamentally, verification of the quantization of the electromagnetic field [8] and insight into different kinds of pair production in spontaneous parametric down-conversion [9, 10].

Four photon entangled states have been observed [11]. Entangled photons produced by parametric down conversion (PDC) are readily shown to obey conservation of angular momentum [12] which has been experimentally shown [13–15]. These high dimensional states have been observed to be entangled experimentally for four photons [16, 17]. Recent publications raise questions about the conversion efficiency in spontaneous versus stimulated emission of photon pairs [8–10].

This thesis investigates the ratio between spontaneous and stimulated PDC pair production, the difference between these two modes is illustrated in Fig. 1.1. To investigate this ratio, a theoretical basis is established. Using the theory previous results are confirmed and expanded upon. Measurements of the dependence of the PDC field intensity on the pump laser power show single pair production in a non-linear crystal.



(a) Two different photon pairs are created by spontaneous emission. These pairs are in a different state and originate from a different place in the crystal.



(b) Two identical photon pairs are created by stimulated emission. These pairs are in the same state.

**Figure 1.1:** In both figures two photon pairs are created. The violet, pulsed laser enters a non-linear crystal. The down-conversion process produces two photon pairs. The green line signifies entanglement of the enclosed photons.

# Chapter 2

## Gaussian Beams

When delving into wave optics, the starting point is at Gaussian beams. These beams describe the way light looks in the paraxial regime. What follows is a summary of relevant results found studying Gaussian beams.

### 2.1 Paraxial Wave Equation

In the paraxial approximation the assumption is valid that the electric field envelope varies slowly in the direction of propagation compared to the other components. This situation is also called the slowly varying envelope approximation. To arrive at the paraxial wave equation for light start with Maxwell's equations in free space,

$$\begin{aligned}\nabla \cdot \mathbf{E} &= 0, & \nabla \cdot \mathbf{B} &= 0, \\ \nabla \times \mathbf{E} &= -\frac{\partial \mathbf{B}}{\partial t}, & \nabla \times \mathbf{B} &= \mu_0 \epsilon_0 \frac{\partial \mathbf{E}}{\partial t}.\end{aligned}$$

Using  $c = \frac{1}{\sqrt{\mu_0 \epsilon_0}}$  and the vector identity  $\nabla \times (\nabla \times \mathbf{F}) = \nabla(\nabla \cdot \mathbf{F}) - \nabla^2 \mathbf{F}$  where  $\mathbf{F}$  is any vector function, the electromagnetic wave equation reveals itself

$$\frac{1}{c^2} \frac{\partial^2 \mathbf{E}}{\partial t^2} - \nabla^2 \mathbf{E} = 0. \quad (2.1)$$

Make the ansatz that the solution is of the form  $\mathbf{E} = U(\mathbf{r})e^{-i\omega t}\hat{\mathbf{n}}$  where  $U$  is a yet to be determined function depending on the position, and  $\hat{\mathbf{n}}$  is the direction of propagation. Then Eq. 2.1 can be written as

$$\frac{\omega^2}{c^2} + \frac{1}{U} \nabla^2 U = 0. \quad (2.2)$$

Using the dispersion relation  $|k| = \omega/c$  this leads to

$$\nabla^2 U + k^2 U = 0, \quad (2.3)$$

which is the Helmholtz equation.

It is useful to write  $U = ue^{ikz}$  where  $z$  is picked to lie along the direction of propagation, implying  $k = k\hat{z}$ . The paraxial approximation assumes  $\theta \ll 1$ , the beam diverges little while propagating along the  $z$ -direction. Let  $\nabla_{\perp}$  denote the nabla operator working the components transverse to the direction of propagation. Using these definitions in Eq. 2.3 leads to

$$\nabla_{\perp}^2 u + \frac{\partial^2 u}{\partial z^2} + 2ik \frac{\partial u}{\partial z} - k^2 u + k^2 u = 0. \quad (2.4)$$

Assuming the slowly varying envelope approximation the rate of change of the  $z$ -component is much smaller than the rate of change in the transverse components;  $|\frac{\partial^2 u}{\partial z^2}| \ll |k \frac{\partial u}{\partial z}|$  and  $\frac{\partial^2 u}{\partial z^2}$  can be dropped. Thus, Eq 2.4 reduces to

$$\nabla_{\perp}^2 u + 2ik \frac{\partial u}{\partial z} = 0. \quad (2.5)$$

A family of solutions to this equation are the Gaussian solutions\*.

## 2.2 Gaussian Solutions

There exist excellent derivations of this solution [18–21], it is not necessary to repeat those here. The Gaussian solution for the electric field is given by

$$E(\rho, z, t) = E_0 \underbrace{\frac{w_0}{w(z)} e^{-\rho^2/w^2(z)}}_{\text{amplitude}} \underbrace{e^{ik(\rho^2)/(2R(z))} e^{-i \arctan\left(\frac{z}{z_R}\right)} e^{i(kz - \omega t)}}_{\text{phase}}. \quad (2.6)$$

In this equation, new parameters arise.  $\rho = \sqrt{x^2 + y^2}$  is the radius in cylindrical coordinates. The  $z$ -coordinate is the distance to the focus. The function  $R(z) = z \left(1 + \left(\frac{z}{z_R}\right)^2\right)$  is the radius of curvature of the wavefront.  $w(z) = w_0 \sqrt{1 + \left(\frac{z}{z_R}\right)^2} = \frac{\text{FWHM}(z)}{\sqrt{2 \ln 2}}$  is the beam size, with the beam waist  $w_0 = w(0)$ .

---

\*Although plane waves are often used as a simplified way to think about light, plane waves are not a solution of the paraxial wave equation.

## 2.3 Hermite-Gauss and Laguerre-Gauss modes

There also exist higher order modes as solutions to the paraxial beam equation. Examples of these are the Hermite-Gauss, Laguerre-Gauss and Ince-Gauss modes. Again, the derivation of these solutions have already been written down in an excellent manner [18, 21]. Below, two of these families of solutions are presented and explained. Both solutions are split up in a part describing the amplitude and a part describing the phase.

### 2.3.1 Hermite-Gauss

The Hermite-Gauss family of solutions is given by

$$E(x, y, z, t) = E_0 \frac{w_0}{w(z)} H_m \left( \frac{\sqrt{2}x}{w(z)} \right) H_n \left( \frac{\sqrt{2}y}{w(z)} \right) e^{(x^2+y^2)/w^2(z)} \quad (2.7)$$

$$\times e^{ik(x^2+y^2)/(2R(z))} e^{-i(m+n+1) \arctan\left(\frac{z}{z_R}\right)} e^{i(kz-\omega t)}.$$

In this expression,  $H_j(x)$  are Hermite polynomials of order  $j \in \mathbb{N}$ . The indices  $m, n \in \mathbb{N}$  signify the order of the mode in the  $x$  and  $y$  directions. These modes show strong symmetry in the cartesian coordinate axes. This is why it is useful to express the solution in terms of cartesian coordinates instead of cylindrical coordinates.

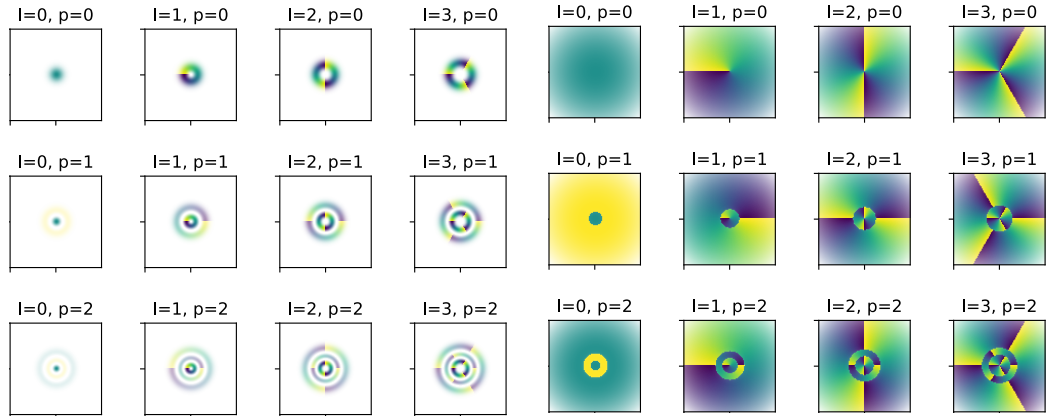
### 2.3.2 Laguerre-Gauss

This family of rotationally symmetric solutions is given in cylindrical coordinates by

$$E(\rho, \phi, z, t) = E_0 \frac{w_0}{w(z)} \sqrt{\frac{2p!}{\pi(p+|\ell|)!}} \left( \frac{\rho\sqrt{2}}{w(z)} \right)^{|\ell|} L_p^{|\ell|} \left( \frac{2\rho^2}{w^2(z)} \right) e^{-\rho^2/w^2(z)}$$

$$\times e^{ik(x^2+y^2)/(2R(z))} e^{-i\ell\phi} e^{-i(|\ell|+2p+1) \arctan\left(\frac{z}{z_R}\right)} e^{i(kz-\omega t)}. \quad (2.8)$$

The expression contains generalized Laguerre polynomials  $L_p^{|\ell|}(x)$  for  $\ell \in \mathbb{Z}$  and  $p \in \mathbb{N}$ . These indices again give rise to different modes which can be seen in Fig. 2.1. Crucially, in these modes the term  $e^{i\ell\phi}$  describing the phase is dependent on the angle coordinate  $\phi$  and an integer  $\ell$ . This  $\ell$  gives rise to orbital angular momentum.



(a) LG-modes plotted using a linear intensity scale.

(b) LG-modes plotted using a logarithmic intensity scale.

**Figure 2.1:** Laguerre-Gauss modes. The color shows the phase, the opacity shows the intensity of the field.

## 2.4 Orbital Angular Momentum

Orbital angular momentum (OAM) may be interpreted as a helix-shaped wavefront. As can be seen in Eq. 2.8,  $\ell$  influences the phase of the beam in the direction of  $\phi$ . Another way to think about this is as a zeroth order (gaussian) wave which is retarded in a spiral fashion. The resulting wavefront has the shape of a helix. The Poynting vector, perpendicular to the wavefront, must then gyrate around the direction of propagation and consequently it imparts angular momentum [22].

# Non-Linear Interactions in a Crystal

In this experiment, photons are entangled in a periodically polled potassium titanyl phosphate (PPKTP) crystal using a process called spontaneous parametric down conversion (SPDC). This process arises from nonlinearities in the field susceptibility of the crystal. An incident photon of wavelength  $\lambda_p$  may result in two photons of wavelength  $\lambda_i$  and  $\lambda_s$  such that energy is conserved:  $1/\lambda_p = 1/\lambda_i + 1/\lambda_s$ . The subscript  $p$  denotes the pump beam while the subscripts  $s, i$  denote the signal and idler field, respectively. They are called signal and idler fields by historical convention, there is no fundamental difference between the two fields. Therefore they will be denoted using the numbers 1 and 2, this will make notation for four photons easier in Ch. 5.

The inverse process where two photons add up to one is called sum frequency generation (SFG). When the two inbound photons have the same wavelength it is called second harmonic generation. SFG is used for various applications in industry, a prime example being cheap laser pointers.

In this chapter the groundwork is laid out to build upon when starting to understand SPDC.

## 3.1 Linear effects

A discussion of linear effects is a stepping stone to higher order effects. The non-linear interactions in anisotropic crystals are the fundamental concepts that will carry over to the description of SFG and SPDC.

Knowledge of the propagation of electric fields in isotropic media is

assumed. The propagation in anisotropic media is discussed further.

### 3.1.1 Permittivity Tensor

For regular materials, the dielectric displacement is related to the electric field by the dielectric constant. In an anisotropic crystal this constant changes depending on the axis through the material considered. Using Einstein summation convention, the electric field  $\mathbf{E}$  and dielectric displacement  $\mathbf{D}$  are now related by a tensor [23, 24]

$$D_k = \epsilon_{kl} E_l \quad (3.1)$$

called the permittivity tensor. This tensor  $\bar{\epsilon}$  is symmetric. To show this, consider the stored electric energy density  $w_e$  of the electric field given by

$$w_e = \frac{1}{2} \mathbf{E} \cdot \mathbf{D} \quad (3.2)$$

$$= \frac{1}{2} E_k \epsilon_{kl} E_l. \quad (3.3)$$

Here, equation 3.1 is used to write the electric displacement in terms of  $\mathbf{E}$ . The time derivative of this energy density is

$$\dot{w}_e = \frac{\epsilon_{kl}}{2} (\dot{E}_k E_l + E_k \dot{E}_l). \quad (3.4)$$

Poynting's theorem relates the net electromagnetic power flow into a unit volume,  $\dot{u}$ , to  $\mathbf{E}$ ,  $\mathbf{D}$ , the magnetic field  $\mathbf{B}$  and the magnetizing field  $\mathbf{H}$  by

$$\dot{u} = \mathbf{E} \cdot \dot{\mathbf{D}} + \mathbf{H} \cdot \dot{\mathbf{B}}. \quad (3.5)$$

Combining above with Eq 3.1 produces

$$\dot{u} = E_k \epsilon_{kl} \dot{E}_l + \mathbf{H} \cdot \dot{\mathbf{B}}. \quad (3.6)$$

The first term on the right side of the equation corresponds to  $\dot{w}_e$  by its definition (the electric energy density) and must be the same as found in Eq. 3.4 [23, 24]. This may be rewritten to

$$\dot{w}_e = \frac{\epsilon_{kl}}{2} (E_k \dot{E}_l + E_l \dot{E}_k) \quad (3.7)$$

Combining Eq. 3.4 and 3.7, the conclusion must be that  $\epsilon_{jk} = \epsilon_{kj}$ . Therefore  $\bar{\epsilon}$  is a symmetric tensor. In three dimensions this leaves six free components.

### 3.1.2 Index Ellipsoid

Explicitly writing out Eq. 3.1 results in

$$2w_e = \epsilon_{xx}E_x^2 + \epsilon_{yy}E_y^2 + \epsilon_{zz}E_z^2 + 2\epsilon_{xy}E_xE_y + 2\epsilon_{xz}E_xE_z + 2\epsilon_{yz}E_yE_z. \quad (3.8)$$

Undergoing a coordinate transformation to diagonalize the electric permittivity tensor this equation becomes

$$2w_e = \epsilon_{xx}E_x^2 + \epsilon_{yy}E_y^2 + \epsilon_{zz}E_z^2 \quad (3.9)$$

where from now on  $x, y, z$  refer to the new coordinate axes, called the principal dielectric axes. All future occurrences of  $x, y$  and  $z$  will be to the principle dielectric axes. Physically, these axes correspond to axes along which  $\mathbf{D}$  and  $\mathbf{E}$  are parallel.

Since the permittivity tensor is now diagonal the double index loses its meaning and, Eq. 3.9 can be written as

$$2w_e = \frac{D_x^2}{\epsilon_x} + \frac{D_y^2}{\epsilon_y} + \frac{D_z^2}{\epsilon_z}, \quad (3.10)$$

as a result the constant energy surface is an ellipsoid in the space  $D_x, D_y, D_z$ . By replacing  $\mathbf{D}/\sqrt{2w_e\epsilon_0}$  with  $\mathbf{r}^*$  and defining the square of the refractive index as  $n_k^2 \equiv \epsilon_k/\epsilon_0$ , this equation becomes the index ellipsoid:

$$\frac{x^2}{n_x^2} + \frac{y^2}{n_y^2} + \frac{z^2}{n_z^2} = 1. \quad (3.11)$$

This index ellipsoid may be used to find the refractive indices corresponding to directions of  $\mathbf{D}$  in the crystal. These indices may be found by finding the normal plane to the direction of propagation and finding the extreme values of the intersection of this plane with the index ellipsoid [24].

### 3.1.3 Linear Electro-Optic Effect

The linear electro-optic (Pockels) effect is a change of the refractive index due to an applied electric field. Suppose a crystal possessing inversion symmetry could harbor the electro-optic effect. Then a change in refractive index  $\Delta n$  would be observed when an electric field is applied, such that  $\Delta n = sE$  for  $s$  some constant characterizing the effect. Reversing the direction of the field, the change in index must be  $\Delta n = s(-E)$ . However,

---

\*This is done to relate to the real space axes in the crystal.

since this crystal has inversion symmetry this should not make a difference for  $\Delta n$ . Thus  $sE = s(-E)$  and either  $s = -s$ , which is not allowed by the symmetry of the crystal, or  $s = 0$ . Only in crystals possessing no inversion symmetry the linear electro-optic effect can exist.

The change in each term of the index ellipsoid can be described by some linear coefficient in each direction of the principal dielectric axes. Letting  $k, l, m \in \{x, y, z\}$ , this change may be written in Einstein notation as

$$\Delta \left( \frac{1}{n^2} \right)_{kl} = r_{klm} E_m. \quad (3.12)$$

The tensor  $\bar{r}$  is the electro-optic tensor. By applying an electric field the index ellipsoid deforms, changing the way electric fields propagate through the material. The change of the refractive index when light passes through gives rise to non-linear behavior.

## 3.2 First Order Non-Linear Effects

The description of SFG and SPDC is impossible with linear effects. To tighten the scope of this thesis, the discussion is limited to non-linearities in the context of either SFG or SPDC. From now on, only SPDC or parametric oscillation will be mentioned since SFG is the inverse process. The description is general enough to apply to SFG [19, 20, 23–27].

Let light of frequency  $\omega_3$  enter the crystal. This wave affects the polarization in the crystal. This does not necessarily happen in a linear fashion, higher order and orthogonal polarization to the inbound electric field may exist. After this non-linear interaction light of frequency  $\omega_1$  and  $\omega_2$  emerges from the other side as a result of this polarization. From energy considerations it can be stated that the frequencies of the emerging light obey the relation  $\omega_3 = \omega_1 + \omega_2$  [19, 20, 23–32].

### 3.2.1 Non-Linear Optical Susceptibility Tensor

The electro-optic tensor from Eq. 3.12 may be related to the polarization of the emerging polarization density field  $P^{\omega_3}$ , defining the nonlinear susceptibility tensor  $\bar{d}$  by

$$P_k^{\omega_3} = d_{klm} E_l^{\omega_1} E_m^{\omega_2}, \quad (3.13)$$

where the tensor  $\bar{d}$  is related to the electro-optic effect by

$$d_{klm} = -\frac{\epsilon_k \epsilon_l}{2\epsilon_0} r_{klm}. \quad (3.14)$$

This is easily derived from the definition of the polarization and Eq. 3.10, 3.11 and 3.12. By relation to  $\bar{r}$  and due to similar arguments for the electric field as presented in Sec. 3.1.3, the nonlinear susceptibility tensor is symmetric in its second and third component. To reflect the restriction on the indices of  $\bar{d}$ , the subscripts  $lm$  can be replaced by the following single index\*

$$\begin{array}{lll} xx = 1 & yy = 2 & zz = 3 \\ yz = zy = 4 & xz = zx = 5 & xy = yx = 6. \end{array}$$

The polarization density can be written as a function of the electric field. Assume the crystal to be very transparent in the frequency range of interest: above the ionic resonance and below electronic absorption. Then the anharmonicity in the restoring force, the second order electric moments and the inelastic photon-lattice scattering interactions are all to be taken negligible compared to non-linear high frequency processes in the crystal [33]. Under these assumptions, the polarization can be considered only a function of the electric field [24].

### 3.2.2 Work

Using the assumptions described above, the contour integral along the edge of an arbitrary region of space is

$$\oint_{\partial C} d(\mathbf{P} \cdot \mathbf{E}) = 0 \quad (3.15)$$

since the electric field is conservative. As a result,

$$-\oint_{\partial C} \mathbf{P} \cdot d\mathbf{E} = \oint_{\partial C} \mathbf{E} \cdot d\mathbf{P}. \quad (3.16)$$

The term on the right is the work done on the polarization by the electric field. Because of our assumption of a 'very transparent' crystal this is zero. Thus, also

$$\oint_{\partial C} \mathbf{P} \cdot d\mathbf{E} = 0. \quad (3.17)$$

Applying Stokes' theorem results in an integral over the electric field through a surface bounded by the contour

$$\oint_{\partial C} \mathbf{P} \cdot d\mathbf{E} = \iint_C (\nabla_E \times \mathbf{P}) \cdot \mathbf{n} dS_E. \quad (3.18)$$

---

\*These indices are not useful to the present discussion, it is mentioned for completeness and to emphasize that the two indices can be reduced to one index, which is used later.

Because the contour integral is zero for an arbitrary surface, applying Stokes' theorem leads to

$$\nabla_E \times \mathbf{P} = 0 \quad (3.19)$$

where  $\nabla_E$  is the nabla operator applied with respect to the components of the electric field. Eq. 3.19 implies the existence of an 'energy' function  $U(\mathbf{E})$  in such a way that

$$\mathbf{P} = -\nabla_E U(\mathbf{E}). \quad (3.20)$$

This 'energy' function is assumed to be at least twice differentiable and thus can be written as a Taylor expansion to at least second order which results in

$$U(\mathbf{E}) = -\frac{\epsilon_0 \chi_{kl}}{2} E_k E_l - \frac{d_{klm}}{6} E_k E_l E_m, \quad (3.21)$$

such that

$$P_k = -\frac{\partial U(\mathbf{E})}{\partial E_k} = \epsilon_0 \chi_{kl} E_l + d_{klm} E_l E_m. \quad (3.22)$$

Note that there is no physical significance attached to the order of  $k, l$  and  $m$ . Therefore all components of  $\bar{d}$  related by a permutation of subscripts are equal to each other, this is called Kleinman's conjecture [24, 33].

The last equation, Eq. 3.22, is made up of two terms. The first term defines  $\bar{\chi}$ , the electric susceptibility. The second term is important to the non-linear effects and is described by the second order electric susceptibility tensor from Sec. 3.2.1. Together they describe the non-linear behavior of the polarization density inside the crystal. Higher order terms are neglected because the given terms describe SPDC without introducing unnecessary complexity.

The way in which non-linear interactions arise in materials has been derived. In the next chapter this theory is explored further to see how it impacts light passing through a non-linear material. It will turn out that non-linearity is the mechanism that causes parametric down-conversion.

# Spontaneous Parametric Down-Conversion

Spontaneous parametric down-conversion is a process which converts one pump photon into two frequency down-converted photons. The quantum state of the crystal is left intact, the down converted photons are only dependent on the pump field. This defines a parametric optical process. Gathering an understanding of SPDC is quite difficult: there is a lot of literature with a qualitative description [19, 20] and a lot of literature with a quantitative description assuming a lot of prerequisite knowledge [9, 13, 34]. In this chapter an attempt will be made to bridge the gap.

This chapter starts with the classical formulation of the nonlinear interaction, this shines some light on fundamental behavior of these interactions. In the first half of this chapter the description is kept as general as possible. A quantum mechanical formulation is introduced. After deriving a general Hamiltonian for SPDC the scope is narrowed down to the paraxial regime.

## 4.1 Classical Formulation

Starting with two of Maxwell's equations in such a way that the polarization  $\mathbf{P}$  is explicit,

$$\nabla \times \mathbf{H} = \mathbf{J} + \frac{\partial \mathbf{D}}{\partial t} = \mathbf{J} + \frac{\partial}{\partial t} (\epsilon_0 \mathbf{E} + \mathbf{P}) \quad (4.1)$$

$$\nabla \times \mathbf{E} = -\frac{\partial}{\partial t} (\mu_0 \mathbf{H}). \quad (4.2)$$

The polarization can be written as a linear and non-linear term according to Sec. 3.2.1,

$$\mathbf{P} = \epsilon_0 \chi_L \mathbf{E} + \mathbf{P}_{\text{NL}}. \quad (4.3)$$

The second order term in the equation relating the electric field to the polarization density (Eq. 3.22) is the non-linear term  $(\mathbf{P}_{\text{NL}})_k = d_{klm} E_l E_m$ . Eq. 4.1 can be written as

$$\nabla \times \mathbf{H} = \bar{\sigma} \mathbf{E} + \frac{\partial}{\partial t} \epsilon \mathbf{E} + \frac{\partial \mathbf{P}_{\text{NL}}}{\partial t} \quad (4.4)$$

using Ohm's law and Eq. 4.3. As is convention,  $\bar{\sigma}$  is the conductivity and  $\epsilon = \epsilon_0(1 + \chi_L)$ .

#### 4.1.1 Equations for three fields

Taking the curl of both sides of Eq. 4.2 and substituting Eq. 4.4 in the resulting equation, one finds

$$\nabla \times \nabla \times \mathbf{E} = -\mu_0 \frac{\partial}{\partial t} \left( \sigma \mathbf{E} + \frac{\partial}{\partial t} \epsilon \mathbf{E} + \frac{\partial \mathbf{P}_{\text{NL}}}{\partial t} \right). \quad (4.5)$$

Since the crystal is neutrally charged on a macroscopic level,  $\nabla \cdot \mathbf{E} = 0$ . Using the vector identity  $\nabla \times \nabla \times \mathbf{F} = \nabla \nabla \cdot \mathbf{F} - \nabla^2 \mathbf{F}$ ,

$$\nabla^2 \mathbf{E} = \mu_0 \sigma \frac{\partial \mathbf{E}}{\partial t} + \mu_0 \epsilon \frac{\partial^2 \mathbf{E}}{\partial t^2} + \mu_0 \frac{\partial^2}{\partial t^2} \mathbf{P}_{\text{NL}}. \quad (4.6)$$

To keep the problem manageable, the problem is limited to one dimension. Set the derivatives in the  $x$  and  $y$  direction to zero and denote the direction of propagation with the  $z$  coordinate. We consider three plane wave fields with frequencies  $\omega_1, \omega_2, \omega_p$  being the idler, signal and pump field, respectively. Each plane wave is of the form

$$E_k^{\omega_i} = \frac{1}{2} (E_{ik}(z) e^{i(\omega_i t - k_i z)} + \text{c.c.}), \quad (4.7)$$

where the index  $k \in \{x, y, z\}$  refers to the coordinates and the label  $i \in \{1, 2, p\}$  selects the wave. The term c.c indicates the complex conjugate of the preceding term. Writing this in components and upon adhering to the previously posed assumptions and restrictions this becomes

$$\nabla^2 E^{\omega_i}(z, t) = \frac{\partial^2}{\partial z^2} E_k^{\omega_i}(z, t) = \frac{1}{2} \frac{\partial^2}{\partial z^2} [E_{ik}(z) e^{i(\omega_i t - k_i z)} + \text{c.c.}]. \quad (4.8)$$

Assuming that the slow varying envelope approximation is valid and after differentiating appropriately

$$\nabla^2 \mathbf{E}^{\omega_i}(z, t) = -\frac{1}{2} \left[ k_i^2 E_{ik}(z) + 2ik_i \frac{dE_{ik}(z)}{dz} \right] e^{i(\omega_i t - k_i z)} + \text{c.c.} \quad (4.9)$$

Finally this may be equated to the right hand side of Eq. 4.6. Moving to frequency space,  $\frac{\partial}{\partial t} \rightarrow i\omega_i$ :

$$\begin{aligned} & \left[ \frac{1}{2} k_i^2 E_{ik} + ik_i \frac{dE_{ik}}{dz} \right] e^{i(\omega_i t - k_i z)} + \text{c.c} \\ &= \left[ -i\omega_i \mu_0 \sigma E_{ik} + \omega_i^2 \mu_0 \epsilon \right] \left[ \frac{E_{ik}}{2} e^{i(\omega_i t - k_i z)} + \text{c.c} \right] + \mu_0 \frac{\partial^2}{\partial t^2} [\mathbf{P}_{\text{NL}}^{\omega_i}(z, t)]_k. \end{aligned} \quad (4.10)$$

Note that if  $\mathbf{P}_{\text{NL}} = 0$  the solution to Eq. 4.6 is given by Eq. 4.7. Otherwise the components of  $\mathbf{P}_{\text{NL}}$  are dependent on the other fields. Namely, consider  $\omega_1 = \omega_p - \omega_2$ . Since the real and imaginary parts of this plane wave phasor are of the same magnitude,

$$E_{p,l} E_{2,m} + E_{p,l}^* E_{2,m}^* = 2 \text{Re}\{E_{p,l}\} \text{Re}\{E_{2,m}\} - 2 \text{Im}\{E_{p,l}\} \text{Im}\{E_{2,m}\} = 0. \quad (4.11)$$

Then the non-linear part of the polarization is given by

$$[\mathbf{P}_{\text{NL}}^{\omega_1}(z, t)]_k = \frac{d_{klm}}{2} E_{p,l}(z) E_{2,m}^*(z) e^{i[(\omega_p - \omega_2)t - (k_p - k_2)z]} + \text{c.c} \quad (4.12)$$

where  $d_{klm}$  is  $\bar{d}$  from Sec. 3.2.1 transformed from the crystal coordinate axes to the axes describing the problem at hand [24].

Combining Eq. 4.10 and 4.12, together with the fact that  $\omega_i^2 \mu_0 \epsilon = k_i^2$  leads to

$$ik_i \frac{\partial E_{1,k}}{\partial z} e^{-ik_1 z} = -\frac{i\omega_1 \sigma \mu_0}{2} E_{1,k} e^{-ik_1 z} + \frac{\mu_0 \omega_1^2}{2} d'_{klm} E_{p,k} E_{2,l}^* e^{-i(k_p - k_2)z}, \quad (4.13)$$

without the loss of generality. Allowing  $\sigma$  to be dependent on  $\omega_i$ , divide by  $ik_1 e^{-ik_1 z}$  to find

$$\frac{\partial E_{1,k}}{\partial z} = -\frac{\sigma_1}{2} \sqrt{\frac{\mu_0}{\epsilon_1}} E_{1,k} - \frac{i\omega_1}{2} \sqrt{\frac{\mu_0}{\epsilon_1}} d'_{klm} E_{p,l} E_{2,m}^* e^{-i(k_p - k_2 - k_1)z}. \quad (4.14)$$

In the same fashion:

$$\frac{\partial E_{2,k}^*}{\partial z} = -\frac{\sigma_2}{2} \sqrt{\frac{\mu_0}{\epsilon_2}} E_{2,k}^* - \frac{i\omega_2}{2} \sqrt{\frac{\mu_0}{\epsilon_2}} d'_{klm} E_{1,l} E_{p,m}^* e^{-i(k_1 - k_p + k_2)z}, \quad (4.15)$$

$$\frac{\partial E_{p,k}}{\partial z} = -\frac{\sigma_p}{2} \sqrt{\frac{\mu_0}{\epsilon_p}} E_{p,k} - \frac{i\omega_p}{2} \sqrt{\frac{\mu_0}{\epsilon_p}} d'_{klm} E_{1,l} E_{2,m} e^{i(k_p - k_2 - k_1)z}. \quad (4.16)$$

These equations describe SPDC classically. The result above follows Yariv [24] and agrees with Couteau [35]. The exponential term leads to an important condition called phase matching which will be discussed in Sec. 4.3. Solving these equations shows energy flowing from the pump field into the signal and idler fields and back; a trick called periodic poling is used to stop energy from flowing back. Periodically poled crystals switch the sign of the non-linear interaction strength. The change of sign is engineered to happen at a depth in the crystal when the direction of energy flow reverses. This is different for every wavelength. Small corrections can be made by changing the temperature of the crystal to slightly change the poling length.

Before moving on to phase matching and periodic poling, it will be useful to consider the quantum mechanical description of SPDC. To derive the quantum Hamiltonian, the classical energy density will be derived first to later quantize in the usual way.

### 4.1.2 Energy density

The work done by the electric field in the crystal per unit time is

$$\frac{dU}{dt} = - \int \mathbf{J} \cdot \mathbf{E} d^3r, \quad (4.17)$$

where the integral is over the volume of the crystal. This is Poynting's theorem in a region of space without field sources or drains\*. Using Eq. 4.1, the current density can be rewritten to  $\mathbf{J} = \nabla \times \mathbf{H} - \frac{\partial \mathbf{D}}{\partial t}$ . Eq. 4.2 is then used to write

$$(\nabla \times \mathbf{H}) \cdot \mathbf{E} = \mathbf{H} \cdot (\nabla \times \mathbf{E}) = -\mathbf{H} \cdot \frac{\partial \mathbf{B}}{\partial t}. \quad (4.18)$$

Making use of this allows Eq. 4.17 to be expressed in terms of fields:

$$\frac{dU}{dt} = \int \left( \mathbf{H} \cdot \frac{\partial \mathbf{B}}{\partial t} + \mathbf{E} \cdot \frac{\partial \mathbf{D}}{\partial t} \right) d^3r. \quad (4.19)$$

Again, the assumption is that the material is very transparent in the frequency range of interest and that the material is non-magnetic such that

$\mu_0 \mathbf{H} = \mathbf{B}$ . Let  $\frac{\epsilon_0 \chi_{klm}^{(2)}}{2} = d_{klm}$ , the equation above can be rewritten to

$$\frac{dU}{dt} = \int \frac{\partial}{\partial t} \left( \mathbf{H} \cdot \mathbf{B} + (\epsilon_0 + \chi) \mathbf{E} \cdot \mathbf{E} \right) d^3r + \frac{\partial}{\partial t} \frac{1}{2} \epsilon_0 \int \chi_{klm}^{(2)} E_k E_l E_m d^3r. \quad (4.20)$$

---

\*The divergence of Poynting's vector is zero;  $\nabla \cdot \mathbf{S} = 0$ . Since the discussion is about propagating fields, this is valid. A down-conversion event respects conservation of energy.

This expression is split into two parts, one describing the usual fields and one describing non-linear interactions. After integrating with respect to time an expression for the energy density is found considering up to second order non-linearity in the polarization. Note that the equation describes a sum over all  $k, l, m$  indices [9, 34].

Since the nonlinear susceptibility is dependent on the frequency of the three fields which is dictated by their respective wave number, the dependence is written explicitly as a sum over its frequency components [34]:

$$\mathcal{H}_{\text{NL}} = \frac{\epsilon_0}{2(\sqrt{2\pi})^3} \int d^3r \sum_{k_1, k_2, k_p} [\chi_{klm}^{(2)}(\omega(\mathbf{k}_1), \omega(\mathbf{k}_2), \omega(\mathbf{k}_p)) \times E_k(\omega(\mathbf{k}_1)) E_l(\omega(\mathbf{k}_2)) E_m(\omega(\mathbf{k}_p))]. \quad (4.21)$$

The factor  $\frac{1}{\sqrt{2\pi}}$  arises from the implicit Fourier transform. This result marks the edge of the classical description and is the stepping stone to a quantum mechanical description of SPDC.

## 4.2 Quantum Hamiltonian

Eq. 4.21 can be quantized to a quantum Hamiltonian consisting of two parts,  $\hat{H} = \hat{H}_L + \hat{H}_{\text{NL}}$ , where the non-linear part is of interest. The linear part is the standard harmonic oscillator hamiltonian for electromagnetic fields [36]. In the non-linear part, replace the electric field by the electric field observable

$$\hat{E}(\mathbf{r}, t) = \hat{E}^+(\mathbf{r}, t) \hat{E}^-(\mathbf{r}, t), \quad (4.22)$$

where  $\hat{E}^-$  is the hermitian conjugate of  $\hat{E}^+$  and [34, 36]

$$\hat{E}^+(\mathbf{r}, t) = \frac{1}{V^{\frac{1}{2}}} \sum_{k,s} i \sqrt{\frac{\hbar\omega(\mathbf{k})}{2\epsilon_0}} \hat{a}_{k,s}(t) \hat{e}_{k,s} e^{i\mathbf{k}\cdot\mathbf{r}}. \quad (4.23)$$

In this equation  $s$  is an index over polarization components,  $V$  is the quantization volume (it goes to infinity in free space),  $\hat{a}_{k,s}(t)$  is the photon annihilation operator at time  $t$  and  $\hat{e}_{k,s}$  is a unit polarization vector. The quantum Hamiltonian takes the form

$$\hat{H}_{\text{NL}} = \frac{1}{2} \epsilon_0 \int d^3r \chi_{klm}^{(2)} \hat{E}_k(\mathbf{r}, t) \hat{E}_l(\mathbf{r}, t) \hat{E}_m(\mathbf{r}, t). \quad (4.24)$$

Since the field operator is a sum of two contributions this Hamiltonian contains eight terms, each term corresponding to a non-linear process. If

the pump beam is sufficiently bright to justify classical treatment and it does not diminish significantly in strength in the crystal, we treat the problem in a regime called the undepleted pump approximation. By considering a single input field and demanding energy conservation under the assumption that this is a parametric process [19, 20, 24–27, 34–38], only two terms are significant:

$$\hat{H}_{\text{NL}} = \frac{1}{2}\epsilon_0 \int d^3r \left( \chi_{klm}^{(2)}(\mathbf{r}) E_k(\mathbf{r}, t) \hat{E}_l^-(\mathbf{r}, t) \hat{E}_m^-(\mathbf{r}, t) + \text{h.c.} \right). \quad (4.25)$$

The term h.c denotes the Hermitian conjugate of the preceding term, analogue to c.c.

Expanding in modes of the three fields,

$$\begin{aligned} \hat{H}_{\text{NL}} = \frac{1}{2}\epsilon_0 \int d^3r \left( \frac{-1}{V} \sum_{k_1, s_1} \sum_{k_2, s_2} \chi_{klm}^{(2)}(\mathbf{r}; \omega(\mathbf{k}_1), \omega(\mathbf{k}_2), \omega(\mathbf{k}_p)) \right. \\ \times \sqrt{\frac{\hbar^2 \omega(\mathbf{k}_1) \omega(\mathbf{k}_2)}{4\epsilon_0^2}} e^{-i(\mathbf{k}_1 + \mathbf{k}_2) \cdot \mathbf{r}} E_k(\mathbf{r}, t) \\ \left. \times \hat{a}_{k_1, s_1}^\dagger(t) \hat{a}_{k_2, s_2}^\dagger(t) (\hat{\mathbf{e}}_{k_1, s_1})_l (\hat{\mathbf{e}}_{k_2, s_2})_m + \text{h.c.} \right) \end{aligned} \quad (4.26)$$

is obtained. Under the assumption that the pump is narrowband, the time dependent part may be separated to good approximation. Further, the pump field is assumed to be well-collimated in order to separate out the longitudinal dependence which is a good approximation. The transverse momenta  $\mathbf{q}_1, \mathbf{q}_2, \mathbf{q}_p$  are the transverse components to the optical axis, and  $k_{1,z}, k_{2,z}, k_{p,z}$  are the parallel components to the optical axis. These vectors are visualized in Fig. 4.1. The polarization vector is defined such that  $E_k(\mathbf{q}_p, t) = \tilde{E}(\mathbf{q}_p, t) (\hat{\mathbf{e}}_{k_p})_k$ . Using these new definitions the pump field may be separated and represented as an integral over plane waves using a Fourier transform:

$$E_k(\mathbf{r}, t) = \frac{1}{2\pi} \int d^2q_p \tilde{E}(\mathbf{q}_p, t) e^{i(\mathbf{q}_p \cdot \mathbf{r})} e^{i(k_z z - \omega_p t)} (\hat{\mathbf{e}}_{k_p})_k. \quad (4.27)$$

Having separated the field like this the Hamiltonian takes the form

$$\begin{aligned} \hat{H}_{\text{NL}} = \frac{1}{4\pi} \epsilon_0 \int d^3r d^2q_p \left( \frac{-1}{V} \sum_{k_1, s_1} \sum_{k_2, s_2} \chi_{klm}^{(2)}(\mathbf{r}; \omega(\mathbf{k}_1), \omega(\mathbf{k}_2), \omega(\mathbf{k}_p)) \right. \\ \times (\hat{\mathbf{e}}_{k_1})_l (\hat{\mathbf{e}}_{k_2})_m (\hat{\mathbf{e}}_{k_p})_k \sqrt{\frac{\hbar^2 \omega(\mathbf{k}_1) \omega(\mathbf{k}_2)}{4\epsilon_0^2}} \\ \left. \times e^{-i(\Delta \mathbf{q}) \cdot \mathbf{r}} e^{-i\Delta k_z r} e^{-i\omega_p t} \tilde{E}_k(\mathbf{r}, t) \hat{a}_{k_1, s_1}^\dagger(t) \hat{a}_{k_2, s_2}^\dagger(t) + \text{h.c.} \right) \end{aligned} \quad (4.28)$$

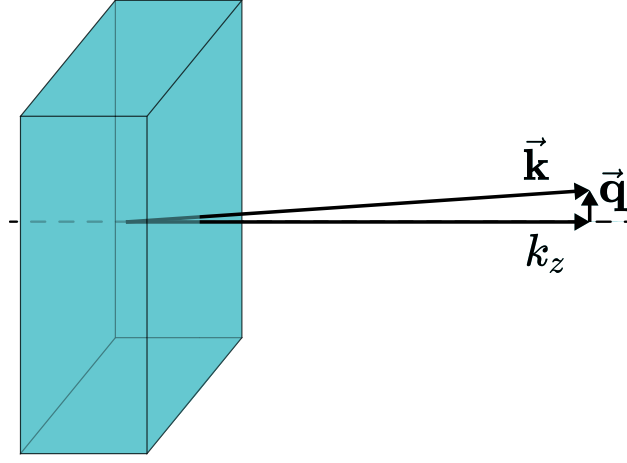


**Figure 4.1:** Schematic drawing of the momentum components of a field coming out of the crystal.

Here,  $\Delta \mathbf{q} = \mathbf{q}_1 + \mathbf{k}_2 - \mathbf{k}_p$  and  $\Delta k_z = k_{1,z} + k_{2,z} - k_{p,z}$  [34].

Now the spatial integral is carried out over the volume of the crystal. In the experiment the anti-reflection coated crystal is approximately rectangular with dimensions  $(L_x, L_y, L_z)$ . Setting bounds from  $-L/2$  to  $L/2$  in each direction, integrating over Cartesian coordinates gives [34, 39]

$$\begin{aligned}
 \hat{H}_{\text{NL}} = \frac{1}{4\pi} \epsilon_0 \int d^2 q_p \left[ \frac{-L_x L_y L_z}{V} \sum_{k_1, s_1} \sum_{k_2, s_2} [\chi_{klm}^{(2)}(\mathbf{r}; \omega(\mathbf{k}_1), \omega(\mathbf{k}_2), \omega(\mathbf{k}_p)) \right. \\
 \times (\hat{\mathbf{e}}_{\mathbf{k}_1})_l (\hat{\mathbf{e}}_{\mathbf{k}_2})_m (\hat{\mathbf{e}}_{\mathbf{k}_p})_k \left. \sqrt{\frac{\hbar^2 \omega(\mathbf{k}_1) \omega(\mathbf{k}_2)}{4\epsilon_0^2}} \right. \\
 \times \text{sinc} \left( \frac{\Delta q_x L_x}{2} \right) \text{sinc} \left( \frac{\Delta q_y L_y}{2} \right) \text{sinc} \left( \frac{\Delta q_z L_z}{2} \right) \\
 \left. \times \tilde{E}(\mathbf{q}_p, t) e^{-i\omega_p t} \hat{\mathbf{a}}_{k_1, s_1}^\dagger(t) \hat{\mathbf{a}}_{k_2, s_2}^\dagger(t) + \text{h.c.} \right].
 \end{aligned} \tag{4.29}$$

Typically, the non-linear part is much weaker than the linear term, this is also true for this experiment. The pump field has a power of about 150 mW and produces not even a  $\mu\text{W}$  of SPDC light. This allows the use of a Taylor expansion to investigate the produced state, resulting in a biphoton wave-function. This is explored in Sec. 4.4.3.

The expression above is a general expression for a SPDC process. The

derivation follows Schneeloch and Howell [34] and agrees with Hong and Mandel [39] who derive the Hamiltonian in a similar manner. For the purposes in this thesis approximations and simplifications will be made in Sec. 4.4. Before assuming specific properties it is useful to first consider phase matching and narrow down the discussion along the way.

### 4.3 Phase Matching

The photon pairs that are created in the non-linear crystal are governed by energy and momentum conservation. Because momentum is a vector it is allowed to point anywhere. Momentum conservation limits the momenta of the down-converted photons to a small component in the transverse direction. Even if all vectors are parallel, which is the collinear case, there can be a difference in momentum due to refractive index dispersion,

$$\Delta k_{\text{coll}} = k(2\omega, T) - 2k(\omega, T) \quad (4.30)$$

$$= \frac{2\omega}{c} (n(2\omega, T) - n(\omega, T)). \quad (4.31)$$

For this reason  $\Delta k_{\text{coll}} \neq 0$  unless the system is carefully engineered [40]. In this equation and the following discussion the case where  $\omega \equiv \omega_1 = \omega_2 = \frac{1}{2}\omega_p$  is considered. It is desired to achieve  $\Delta k_{\text{coll}} \sim 0$  to maximize the output of non-linear processes, this condition is called phase matching. One way to achieve phase matching exploits the birefringence of the crystal, appropriately called birefringent phase matching [41]. Another possibility is quasi-phase matching, realized by periodic poling [42, 43]. This is discussed below in detail as it is used in the experiment.

#### 4.3.1 Periodic Poling

From a classical viewpoint, the equations describing the main result in Sec. 4.1 can be solved for the equivalent case of SFG with equal wavelength of the incident photons: second harmonic generation (SHG). This process can be seen as the inverse process of SPDC. We take Eq. 4.16 and assume the degenerate case,  $\omega_p = 2\omega$ , in the undepleted pump approximation. Since the degenerate case is considered, the signal and idler fields ( $E_1$  and  $E_2$ ) are treated the same. The outgoing field (what would be the pump field in SPDC, therefor labeled with the index ' $p$ ') is

$$\frac{dE_{p,l}}{dz} = -i\omega \sqrt{\frac{\mu_0}{\epsilon_3}} d'_{klm} E_{1,k} E_{1,m} e^{i\Delta kz} \quad (4.32)$$

which, upon integrating over a crystal length  $L$  and with  $\Delta k$  as in Eq. 4.30 leads to

$$E_{3,l}(L) = -i\omega \sqrt{\frac{\mu_0}{\epsilon_3}} d'_{klm} E_{1,k} E_{1,m} \frac{e^{i\Delta k z} - 1}{i\Delta k}. \quad (4.33)$$

The power of the produced photons is proportional to

$$E_{3,l} E_{3,l}^* = \frac{\mu_0}{\epsilon_3} \omega^2 (d'_{klm})^2 E_{1,k}^2 E_{1,m}^2 L^2 \text{sinc}^2(\Delta k L / 2). \quad (4.34)$$

In the derivation of the quantum Hamiltonian the sinc term arises from the Fourier transform over the rectangular crystal, in the classical case (above) it comes from the integral over the crystal length. In Sec 4.4.3 it is shown that the sinc function is also present in the biphoton wavefunction [24, 44].

Equation 4.34 reveals that the efficiency of this process is limited by the term  $\text{sinc}^2(\Delta k L / 2)$ . The distance between two adjacent peaks defines the coherence length  $l_c$  [24]. It is a measure for the maximum crystal length after which the power output becomes zero again. The reason that this happens is that the output wave can get out of phase with the pump wave, power can flow back into back into it [38]. As in the classical analysis, by inverting the non-linear electrical susceptibility after this length the power can keep on increasing. Doing this over and over is called periodic poling [43, 45].

The switching of the non-linear susceptibility can be shown mathematically to contribute a vector  $k$  to the phase matching parameter \* [38, 46]. By tuning this reciprocal lattice vector phase matching may be achieved. The contributing reciprocal lattice vector is  $k = \frac{2\pi}{\Lambda}$  where the poling period  $\Lambda$  is twice the coherence length,  $\Lambda = 2l_c$  [40]. With this addition,

$$\Delta k = \frac{2\omega}{c} (n(2\omega, T) - n(\omega, T)) - \frac{2\pi}{\Lambda}, \quad (4.35)$$

which can be tuned to  $\Delta k \sim 0$ .

## 4.4 Structure of SPDC Light

Light emitted from the SPDC process is divergent. This is due to the fact that the wave vectors are, in general, not collinear. As made clear in Fig.

---

\*The approach is to switch the sign of the electric susceptibility by modeling it as a square wave, then take the Fourier transform. Substituting the modulated electric susceptibility in Eq. 4.14 – 4.16 produces an extra term  $k$ , leading to  $\Delta k$  as defined in Eq. 4.35. This approach is worked out in [38, Ch. 2.4].

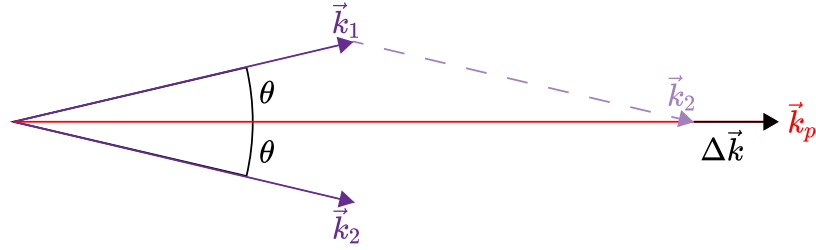


**Figure 4.2:** Vector sum of  $\Delta k$  in the non-collinear case.  $k_1$  and  $k_2$  add up to  $k_p - k$  as in Eq. 4.35. Phase matching is achieved in this situation. Both  $k_1$  and  $k_2$  make an angle  $\theta$  with the optical axis.

4.2, the vector sum as described in Eq. 4.35 has transverse components and thus the signal and idler photons come out of the crystal at an angle  $\theta$  to the optical axis (chosen parallel with the pump beam). Geometrically this angle can thus be linked to the phase matching condition allowing an expression for the half-angle divergence of the degenerate SPDC light. Note that this angle is typically small.

#### 4.4.1 Half-angle divergence of degenerate SPDC light

Letting  $\Delta k_z$  be the phase mismatch in the  $z$ -component while not taking periodic poling into account. The relation

$$k_p = (k_1 + k_2) \cos(\theta) - \Delta k_z \quad (4.36)$$

is found from conservation of momentum in the  $z$ -direction as is evident from Fig. 4.2. Since the degenerate case is considered,  $k_1 = k_2 = \frac{1}{2}k_p$ . Using the small angle approximation

$$\Delta k = -\frac{1}{2}\theta^2 k_p. \quad (4.37)$$

In Eq. 4.34 the sinc term is dependent on  $\Delta k$ , this can be used to find the half-angle divergence of the SPDC light by finding the distance to the first minimum of the sinc function. This minimum is located at  $\text{sinc}^2(\pm\pi) = 0$ . Thus

$$\theta = \sqrt{\frac{2\lambda_p}{L_z}}, \quad (4.38)$$

where the relation  $\lambda_p = \frac{2\pi}{k_p}$  is used.

### 4.4.2 Klyshko Picture

The Advanced Wave Picture (AWP) was pioneered by Klyshko [47] as a way to describe non-classical interference effects. This method has been applied to SPDC often with good results [48, 49]. The idea is to pretend that one detector emits a wave towards the crystal, which reflects from the pump beam's wave-fronts\* towards the other detector. In this way information can be gained about the system. This method also proved useful for simulating correlations in OAM of down converted photons [50].

### 4.4.3 Degenerate Collinear Bi-photon Wave Function

The bi-photon wave function can be used as an expression for the angular distribution of the down converted field. Again, we assume the degenerate case in the undepleted pump approximation and type-I down conversion; the polarization of the signal and idler photons are the same and orthogonal to the pump photons.

In the interaction picture, the bi-photon wave function can be approximated as it evolves through the crystal as the first order correction obtained from time-dependent perturbation theory:

$$|\psi(t)\rangle = -\frac{i}{\hbar} \int_0^t dt' \hat{H}_{\text{NL}}(t') |\psi(0)\rangle. \quad (4.39)$$

Because we are considering type-I down-conversion the sum over the polarization states in Eq. 4.29 may be neglected. The terms concerning SHG are also dropped. Then the non-linear susceptibility is a single value which is expressed as  $\chi_{\text{eff}}^{(2)}$ . Further assuming that the crystal is much longer than the wavelength of both the pump and the down converted fields, the sum over the wave vectors can be replaced by an integral:

$$\lim_{V \rightarrow \infty} \frac{1}{V} \sum_{\mathbf{k}_i} \longrightarrow \frac{1}{(2\pi)^3} \int d^3 k_i. \quad (4.40)$$

Then the non-linear Hamiltonian can be written as

$$\begin{aligned} \hat{H}_{\text{NL}} &\approx C_{\text{NL}} \chi_{\text{eff}}^{(2)} \int \int d^3 k_1 d^3 k_2 \sqrt{\omega(\mathbf{k}_1) \omega(\mathbf{k}_2)} \\ &\times \int d^2 q_p \left[ \prod_{m \in \{x, y, z\}} \text{sinc} \left( \frac{\Delta k_m L_m}{2} \right) \right] \tilde{E}(\mathbf{q}_p, t) e^{i\Delta\omega t} \hat{a}^\dagger(\mathbf{k}_1) \hat{a}^\dagger(\mathbf{k}_2). \end{aligned} \quad (4.41)$$

---

\*In effect, the crystal can be replaced by a curved mirror matching the pump beam wave fronts.

$C_{\text{NL}}$  is a constant absorbing some terms from Eq. 4.29 and  $\Delta\omega \equiv \omega_1 + \omega_2 - \omega_p$ . To condense the notation let  $\Delta q_{x(y)} = \Delta k_{x(y)}$  [34].

Since we are considering the undepleted pump approximation, the pump field can be written as a constant times a Gaussian times  $e^{i\omega_p t}$ . This time dependence is already contained in the term with  $\Delta\omega$ . Then the integral resulting in the first order contribution can be evaluated, resulting in

$$\begin{aligned} |\psi_{\text{SPDC}}^{(1)}\rangle &= C_1 \chi_{\text{eff}}^{(2)} \sqrt{I_p T^2} \int \int d^3 k_1 d^3 k_2 \Phi(\mathbf{k}_1, \mathbf{k}_2) \\ &\times \sqrt{\omega(\mathbf{k}_1)\omega(\mathbf{k}_2)} e^{\frac{i\Delta\omega t}{2}} \text{sinc}\left(\frac{\Delta k_m L_m}{2}\right) \hat{a}^\dagger(\mathbf{k}_1) \hat{a}^\dagger(\mathbf{k}_2) |0_1, 0_2\rangle. \end{aligned} \quad (4.42)$$

In the equation above,  $T$  is the time it takes for the light to propagate through the crystal,  $I_p$  is the intensity of the pump beam and the Hamiltonian is applied to the vacuum state of the idler and signal photons:  $|0_1, 0_2\rangle$ . Finally, the bi-photon wave function \* reveals itself:

$$\Phi(\mathbf{k}_1, \mathbf{k}_2) = \int d^2 q_p \left[ \prod_{m \in \{x, y, z\}} \text{sinc}\left(\frac{\Delta k_m L_m}{2}\right) \right] \nu(\mathbf{q}_p), \quad (4.43)$$

with  $\nu(\mathbf{q}_p)$  the normalized pump amplitude spectrum. This expression is however not normalized. Still, Eq. 4.42 indicates how the first order contributions scale in the photon count rate [51],

$$R_{\text{SPDC}} \propto \chi_{\text{eff}}^2 P_p L_z^2 \quad (4.44)$$

The pump laser used in the experiment has  $\text{sech}^2$ -shaped pulses in the frequency domain. This  $\text{sech}^2$ -shaped frequency distribution [52] is approximated by a Gaussian pulse [53] such that<sup>†</sup>

$$\nu(\mathbf{q}_p) = \left(\frac{2\sigma_p^2}{\pi}\right)^{\frac{1}{4}} e^{-\sigma_p^2 |\mathbf{q}_p|^2}. \quad (4.45)$$

The momentum of the pump is the sum of the momenta of the signal and idler beams,  $\mathbf{q}_p = \mathbf{q}_1 + \mathbf{q}_2$ . Because  $\Delta k_{y(z)} \sim 0$ , the sinc functions in the  $y$  and the  $z$  component of Eq. 4.43 will effectively act like delta functions

\*Note that  $\Phi(\mathbf{k}_1, \mathbf{k}_2)$  does not evolve according to the Schrödinger equation; it says something about the field coming out of the crystal. The whole of  $|\psi_{\text{SPDC}}\rangle = C_0 |0_1, 0_2\rangle + |\psi_{\text{SPDC}}^{(1)}\rangle$  does evolve appropriately.

<sup>†</sup>This approximation is pretty good. The  $\text{sech}$  shaped pulse has broader wings, however with a smaller time-bandwidth product.

[34]. With normalization constant  $\mathcal{C}$  the bi-photon wave function is obtained:

$$\Phi(\mathbf{k}_1, \mathbf{k}_2) = \mathcal{C} \operatorname{sinc}\left(\frac{\Delta k_z L_z}{2}\right) e^{-\sigma_p^2 |\mathbf{q}_1 + \mathbf{q}_2|^2}. \quad (4.46)$$

An expression for  $\Delta k_z$  needs to be derived in order for this expression to be useful.

### Coordinate transformation

Using Eq. 4.36 and momentum conservation in the transverse direction:

$$\frac{|\mathbf{q}_1 - \mathbf{q}_2|}{2} = k_1 \sin(\theta), \quad (4.47)$$

an expression can be found for  $\Delta k$  in terms of the transverse components. Making use of the small angle approximation and the degeneracy, meaning  $k_1 = k_2 = \frac{1}{2}k_p$ , we obtain

$$k_p \approx (k_1 k_2) \left(1 - \frac{1}{2}\theta^2\right) - \Delta k \quad (4.48)$$

$$\theta \approx \frac{|\mathbf{q}_1 - \mathbf{q}_2|}{k_p}. \quad (4.49)$$

Substituting one of these intermediate results in the other results in [34]

$$\Delta k \approx -\frac{|\mathbf{q}_1 - \mathbf{q}_2|^2}{2k_p}. \quad (4.50)$$

This can be inserted in Eq. 4.46. The bi-photon wave function becomes [54]

$$\Phi(\mathbf{q}_1, \mathbf{q}_2) = \frac{\sigma_p}{\pi^2} \sqrt{L_z \lambda_p} \operatorname{sinc}\left(\frac{L_z \lambda_p}{8\pi n_p} |\mathbf{q}_1 - \mathbf{q}_2|^2\right) e^{-\sigma_p^2 |\mathbf{q}_1 + \mathbf{q}_2|^2}, \quad (4.51)$$

where the constant  $\mathcal{C}$  is calculated by normalizing the function.

Now a coordinate transformation can be made:

$$\mathbf{q}_+ = \frac{\mathbf{q}_1 + \mathbf{q}_2}{\sqrt{2}}, \quad \mathbf{q}_- = \frac{\mathbf{q}_1 - \mathbf{q}_2}{\sqrt{2}}.$$

In this coordinate system,

$$\Phi(\mathbf{q}_+, \mathbf{q}_-) = \frac{\sigma_p}{\pi^2} \sqrt{L_z \lambda_p} \operatorname{sinc}\left(\frac{L_z \lambda_p}{8\pi n_p} |\mathbf{q}_-|^2\right) e^{-\sigma_p^2 |\mathbf{q}_+|^2}. \quad (4.52)$$

Writing the expression in this coordinate system separates the terms.

### Near Field

The near field is given by  $\Phi^*\Phi$  in  $k$ -space, as that results in a probability distribution of the down-converted field. Thus,

$$|\Phi(\mathbf{q}_1, \mathbf{q}_2)|^2 = \frac{\sigma_p^2}{\pi^4} L_z \lambda_p \operatorname{sinc}^2 \left( \frac{L_z \lambda_p}{8\pi n_p} |\mathbf{q}_1 - \mathbf{q}_2|^2 \right) e^{-2\sigma_p^2 |\mathbf{q}_1 + \mathbf{q}_2|^2}. \quad (4.53)$$

This result makes sense, the biphoton wave function can be interpreted as the photon quasi-probability distribution [34]. In that sense, the field must be the square of the quasi-probability distribution.

### Far Field

Since measurements are done in the far field and the LG-modes are described in spatial coordinates, it is useful to write the biphoton wave function in a spatial basis. Later this will prove useful when decomposing the wave function to LG-modes.

The far field is related to the near field by a Fourier transform. This is best done in the rotated coordinate system, however the Fourier transform of  $\operatorname{sinc}(ax^2)$  is tricky. Therefore it is approximated by a Gaussian.

The procedure is to calculate the first and second moment of the expectation value of the probability density for  $\mathbf{q}_-$  and to fit that to a Gaussian. This is easily Fourier transformed. To read up on the details of this approximation please refer to Chapter IV of [34]. The result is consequently shaped as a Gaussian.

In a paper by Walborn a more precise solution is given [54]. In the paraxial approximation and ignoring detuning from the target frequency\* the field operator is proportional to

$$\hat{E}(\boldsymbol{\rho}, z, t) \propto e^{i(kz)} \int d\Omega d\mathbf{q} e^{i\left(\mathbf{q} \cdot \boldsymbol{\rho} - \frac{q^2 z}{2k}\right)} \hat{a}(\mathbf{q}, \Omega). \quad (4.54)$$

For two photons the spatial wave function can be calculated by using the electric field operators at positions  $\mathbf{r}_1$  and  $\mathbf{r}_2$  and applying the resulting

---

\*The PPKTP crystal performs best at a set wavelength. The detuning refers to the difference in frequency of the fields from this wavelength, it takes into account the finite bandwidth of the fields.

state to the vacuum state bra\* [54]

$$\begin{aligned}\Theta^{II}(\boldsymbol{\rho}_1, \boldsymbol{\rho}_2) &= \langle vac | \hat{E}_1(\mathbf{r}_1) \hat{E}_2(\mathbf{r}_2) | \mathbf{q}_1, \mathbf{q}_2 \rangle \\ &= \int_{\mathbb{R}^4} d\mathbf{q}_1 d\mathbf{q}_2 e^{i\left(\mathbf{q}_1 \cdot \boldsymbol{\rho}_1 + \mathbf{q}_2 \cdot \boldsymbol{\rho}_2 - \frac{(q_1^2 + q_2^2)z}{2k}\right)} \times \phi(\mathbf{q}_1, \mathbf{q}_2).\end{aligned}\quad (4.55)$$

The result of the procedure can be seen as a Fourier transform multiplied by a phase factor accounting for propagation. This factor takes non-collinear phase matching into account in the paraxial regime. By writing Eq. 4.55 in the rotated coordinate basis the integral can be split up into a part describing the pump beam and a part describing the phase matching function. The result is the spatial description of the pump beam, to broaden the discussion a general LG-mode is chosen. The transformed biphoton wave function is [54]<sup>†</sup>

$$\Theta^{II}(\boldsymbol{\rho}_1, \boldsymbol{\rho}_2) = LG_{p_p}^{\ell_p} \left( \frac{\boldsymbol{\rho}_1 + \boldsymbol{\rho}_2}{2} \right) \frac{\sqrt{L_z k_p}}{2\pi z} \text{sinc} \left( \frac{L_z k_p}{8z^2} \frac{|\boldsymbol{\rho}_1 - \boldsymbol{\rho}_2|^2}{2} \right). \quad (4.56)$$

For simplicity, it is assumed that  $z_1 = z_2 = z$ . As the field propagates, the sinc function spreads out. This is simply the broadening of the field on propagation and is a manifestation of the uncertainty principle.

In this section we have derived our main result: the bi-photon wave function. This is a real, symmetric function of two coordinates. It describes the behavior of two photons in the PDC process. It is not actually a wave function (it does not evolve correctly under the Schrödinger equation on its own), it describes the state of the two photons. The bi-photon wave function is a wave function in the sense that the absolute square of this function returns a probability distribution.

## 4.5 Conservation of Orbital Angular Momentum

The bi-photon wave function (Eq. 4.43) can be written by Schmidt decomposition in terms of OAM modes [55]. This is a beautiful result where mathematics and physics come together.

---

\*The resulting expression is obtained through the same method outlined in Appx. A. The method relies on using the commutation relation to place the creation and annihilation operators in normal order. To apply the method here, it is important to realize that  $|\mathbf{q}_1, \mathbf{q}_2\rangle = \phi(\mathbf{q}_1, \mathbf{q}_2) \hat{a}^\dagger(\mathbf{q}_1) \hat{a}^\dagger(\mathbf{q}_2) |vac\rangle$ .

<sup>†</sup>Because it is more useful for the upcoming analysis the equation is written in terms of  $k = \frac{2\pi n}{\lambda}$ , notice the dependence of  $k$  on the refractive index.

### 4.5.1 Schmidt Decomposition and Schmidt Number

The Schmidt decomposition theorem can be stated as: [36]

**Theorem 1** Let  $\mathcal{H}_1, \mathcal{H}_2$  be Hilbert spaces of dimensions  $n$  and  $m$  respectively where it is assumed that  $n \geq m$ . For any  $w \in \mathcal{H}_1 \otimes \mathcal{H}_2$  there exists orthonormal bases  $u_1, \dots, u_m \in \mathcal{H}_1, v_1, \dots, v_m \in \mathcal{H}_2$  such that

$$w = \sum_{i=1}^m \sqrt{\lambda_i} u_i \otimes v_i \quad (4.57)$$

where the scalar coefficients  $\lambda_i$  are uniquely determined by  $w$  and are larger or equal to zero.

The Schmidt number is defined in Law and Eberly as  $K \equiv 1 / \sum_n \lambda_n^2$  [55]. This ‘average’ is a measure for the ‘amount of entanglement’; if there is one term in the decomposition  $w$  can be written as a product, then the state is not entangled. If the state can not be written as a product the state is entangled. For higher  $w$  it is more difficult to write the function as a Schmidt decomposition: more terms are needed. This can be interpreted as ‘more entangled’.

### 4.5.2 Decomposition of the Biphoton Wavefunction

The Schmidt decomposition can be applied to Eq. 4.51. Using the gaussian-sinc approximation this can be calculated analytically [56], in an influential paper by Law and Eberly [55] it was first explained to be possible in the general case.

We start by writing the transverse momentum in polar coordinates,

$$\mathbf{q}_{1(2)} = (q_{1(2)} \cos(\theta_{1(2)}), q_{1(2)} \sin(\theta_{1(2)})). \quad (4.58)$$

There will exist a decomposition such that [55]

$$\phi(\mathbf{q}_1, \mathbf{q}_2) = \sum_{n=0}^{\infty} e^{im(\theta_1 - \theta_2)} \sqrt{P_m} F_m(q_1, q_2) / (2\pi). \quad (4.59)$$

This can once again be written as a Schmidt decomposition resulting in [55]

$$\phi(\mathbf{q}_1, \mathbf{q}_2) = \sum_{m=-\infty}^{\infty} \sum_{n=-\infty}^{\infty} \sqrt{\lambda_{n,m}} u_{n,m}(q_1) u_{n,-m}(q_2), \quad (4.60)$$

where

$$u_{n,m}(\mathbf{q}_{1(2)}) \equiv \frac{e^{im\theta_{1(2)}}}{\sqrt{2\pi q_{1(2)}}} \psi_{n,m}(q_{1(2)}). \quad (4.61)$$

The function  $\psi_{n,m}$  should be chosen in a clever way. Because OAM is of interest, let  $e^{im\theta} \psi_{n,m}$  equal the generalized Laguerre polynomial in mode  $n, m$  to define  $\psi_{n,m}$ . Using this, the coefficient  $\lambda_{n,m}$  can be calculated numerically [57].

The emerging term  $e^{im(\theta_1 - \theta_2)}$  is the cause of the sign of  $m$  in  $u_{n,m}$  and  $u_{n,-m}$ . Due to the way the bases are chosen  $m$  can be interpreted as OAM. As a result OAM is a conserved quantity; the spiral modes need to add up in such a way that Eq. 4.60 holds. Walborn et al. [54] have proven that this can not be explained classically; the correlations found in the coefficients are a quantum effect.

### 4.5.3 Calculating the Coefficients

Using a similar procedure as in the previous section the spatial wave function (Eq. 4.56) can be decomposed. This is an easier path to results because the LG-modes are described spatially. The decomposition is

$$|\Psi(\boldsymbol{\rho}_1, \boldsymbol{\rho}_2)\rangle = \sum_{\ell_1, \ell_2, p_1, p_2} C_{\ell_1, \ell_2}^{p_1, p_2} \text{LG}_{p_1}^{\ell_1}(\boldsymbol{\rho}_1) \text{LG}_{p_2}^{\ell_2}(\boldsymbol{\rho}_2). \quad (4.62)$$

The Schmidt coefficients for two photons can be calculated using

$$C_{\ell_1, \ell_2}^{p_1, p_2} = \int_{\mathbb{R}^4} d\boldsymbol{\rho}_1 d\boldsymbol{\rho}_2 \text{LG}_{p_1}^{*\ell_1}(\boldsymbol{\rho}_1) \text{LG}_{p_2}^{*\ell_2}(\boldsymbol{\rho}_2) \Theta^{II}(\boldsymbol{\rho}_1, \boldsymbol{\rho}_2). \quad (4.63)$$

In the thin-crystal limit the phase matching function can be approximated to one. Even for large combinations of  $|\ell|$  and  $p$  the approximation is accurate to 1% [54]. The coefficients are then calculated by evaluating the integrals

$$C_{\ell_1, \ell_2}^{p_1, p_2} = \int_{\mathbb{R}^4} d\boldsymbol{\rho}_1 d\boldsymbol{\rho}_2 \text{LG}_{p_1}^{*\ell_1}(\boldsymbol{\rho}_1) \text{LG}_{p_2}^{*\ell_2}(\boldsymbol{\rho}_2) \text{LG}_{p_p}^{\ell_p} \left( \frac{\boldsymbol{\rho}_1 + \boldsymbol{\rho}_2}{\sqrt{2}} \right). \quad (4.64)$$

The spatial coordinates for the pump beam arise from the fact that up to a phase factor and normalization constant [54]

$$\mathcal{E}(\boldsymbol{\rho}; \lambda_0, w_0) = \mathcal{E}(\sqrt{2}\boldsymbol{\rho}; 2\lambda_0, \sqrt{2}w_0) = \text{LG}(\sqrt{2}\boldsymbol{\rho}). \quad (4.65)$$

This equality makes use the down-converted fields possessing half the frequency as the pump field (thus  $\lambda_1 = \lambda_2 \equiv \lambda$ ) and consequently using the similarity of the LG-modes. The coefficients are now expressed as an integral over orthogonal modes.

#### 4.5.4 Explicitly Showing Conservation of OAM

While it is not directly obvious from the form of Eq. 4.64, OAM is conserved. This can be made explicit by using a coordinate transformation as in Sec. 4.4.3 and a Fourier transform, as Walborn showed [54]. Let  $\text{FLG}_p^\ell(\mathbf{q})$  be the Fourier transform of a Laguerre-Gauss mode. With these changes, Eq. 4.64 can be written as

$$C_{\ell_1, \ell_2}^{p_1, p_2} \propto \int d\rho_+ dq dq' \text{FLG}_{p_1}^{*\ell_1}(\mathbf{q}) \text{FLG}_{p_2}^{*\ell_2}(\mathbf{q}) \text{FLG}_{p_p}^{\ell_p}(2\mathbf{q}') \times e^{i\rho_+(q'-q)} \quad (4.66)$$

$$\propto \int d\mathbf{q} \text{FLG}_{p_1}^{*\ell_1}(\mathbf{q}) \text{FLG}_{p_2}^{*\ell_2}(\mathbf{q}) \text{FLG}_{p_p}^{\ell_p}(2\mathbf{q}). \quad (4.67)$$

To separate out the spiral term, let  $\text{Flg}_p^\ell(\mathbf{q})e^{i\ell\phi} = \text{FLG}_p^\ell(\mathbf{q})$ . Then, the equation above can be written as

$$C_{\ell_1, \ell_2}^{p_1, p_2} \propto \iint q dq d\phi \text{Flg}_{p_1}^{*\ell_1}(\mathbf{q}) \text{Flg}_{p_2}^{*\ell_2}(\mathbf{q}) \text{Flg}_{p_p}^{\ell_p}(2\mathbf{q}) e^{i(\ell_p - \ell_1 - \ell_2)\phi} \quad (4.68)$$

$$\propto \delta_{\ell_p, \ell_1 + \ell_2} \int q dq \text{Flg}_{p_1}^{*\ell_1}(\mathbf{q}) \text{Flg}_{p_2}^{*\ell_2}(\mathbf{q}) \text{Flg}_{p_p}^{\ell_p}(2\mathbf{q}). \quad (4.69)$$

The term  $\delta_{\ell_p, \ell_1 + \ell_2}$  explicitly shows conservation of orbital angular momentum.

In this chapter, SPDC was presented using both a classical and quantum description. This is important for understanding what goes on in the crystal and what processes happen. Important results are the bi-photon wave function (Eq. 4.43), the spatial bi-photon wave function (Eq. 4.56) and the conservation of OAM for single photon pairs (Eq. 4.69). In the next chapter these results will be used in the discussion of double photon pairs.

## Four Photon Type-I PDC

In Ch. 4 the theory of SPDC is explained. The Hamiltonian derived will be applied to the case of high pump laser power.

At high pump laser powers stimulated emission can occur, much like the principle upon which lasers rest. A passing photon pair can stimulate the emission of an identical pair. This is contrary to a spontaneous pair which is created without influence of radiation in the same mode\*. This is why we now refer to the down-converted field as the PDC field, it is not necessarily spontaneous.

This section rests on assumptions and simplifications. One is the undepleted pump approximation; the pump field is taken to be much stronger than the signal and idler fields. If this is true, the pump field can be regarded as a classical field that does not diminish in intensity as it passes through the crystal. Further, in the experiment type-I SPDC is used<sup>†</sup>. The signal and idler beams have the same polarization, therefore the polarization does not matter for the PDC process and is ignored in the Hamiltonian. Another important approximation is that the non-linear Hamiltonian is small relative to the EM-field Hamiltonian (the second term in Eq. 4.20 is much smaller compared to the first term). The system is engineered to consider collinear phase-matching tuned to a point where the PDC field is shaped like a Gaussian and not like a ring [25, 26]. This is true in the

---

\*It is possible to stimulate these emissions by using a second incident laser in the desired mode.

<sup>†</sup>There are three types of SPDC. In Type-0 SPDC the pump and down-converted photons share the same polarization. In Type-1 SPDC the pump and down-converted photons have orthogonal polarizations, the outgoing photons share the same polarization. In Type-II SPDC the two outgoing photons have orthogonal polarizations. In this experiment the crystal only allows Type-I PDC.

paraxial regime, which is another assumption. Finally, a thin crystal is assumed without taking the thin crystal limit.

## 5.1 Spontaneous or Stimulated Emission?

For high pump laser intensities, the PDC process can happen multiple times in a single laser pulse. One possibility is that a photon pair is created, independent from the previously created pair. This is called spontaneous emission. Stimulated emission is also possible; a second pair is created having the exact same properties of the first photon pair. In this case, the two pairs are entangled. These states are of interest. It is therefore important to be able to distinguish them and to optimize the stimulated emission process.

The probability of creating two independent pairs is  $P_4 \approx P_2^2/2$ , half of the square of the probability of creating two photons [58]. The probability of creating two entangled pairs is  $P_4 = P_2^2$ , the emission of the second pair is due to the existence of the first pair. The system will behave somewhere between these two extremes. It is useful to characterize it with the visibility,  $\chi \in [0, 1]^*$

$$P_4 = \frac{P_2^2}{2}(1 + \chi). \quad (5.1)$$

This parameter is a measure for the extra contribution of the stimulated emission [59]. It is dependent on the coherence length of the PDC light and the pulse length of the pump.

## 5.2 Approximation of the PDC State

The Hamiltonian derived in Sec 4.2 is  $\hat{H} = \hat{H}_L + \hat{H}_{NL}$ , the last term is given by equation 4.29. The non-linear part dictates the interaction during the propagation through the crystal. This interaction produces the wave function describing the down-converted field: the PDC state. In this experiment the PDC state is in the collinear regime, the system is engineered in this way. The temperature of the crystal slightly changes the periodic polling length. The length is adjusted to guarantee a PDC field with small transverse momenta.

---

\*Though sharing the same symbol, it is not to be confused with the electric susceptibility.

### 5.2.1 Momentum Basis

In the Schrödinger picture, the time evolution of a quantum state is governed by

$$|\psi(t)\rangle = e^{\frac{\hat{H}t}{\hbar}} |\psi(0)\rangle, \quad (5.2)$$

which may be expressed as a Taylor expansion up to second order in terms of  $\frac{\hat{H}t}{\hbar}$  as

$$|\psi(t)\rangle \approx \left(1 - \frac{i}{\hbar}\hat{H}t - \frac{1}{2}\frac{1}{\hbar^2}\hat{H}^2t^2\right) |\psi(0)\rangle. \quad (5.3)$$

In the experiment this approximation is justified by the small power of the SPDC light. The pair production probability is around  $10^{-9}$  [34], the non-linear Hamiltonian is truly very small.

Written in a more explicit way

$$|\psi\rangle = A |vac\rangle + B |\psi^{(1)}\rangle + C |\psi^{(2)}\rangle \quad (5.4)$$

where

$$|\psi^{(1)}\rangle = \iint d\mathbf{q}_1 d\mathbf{q}_2 \phi(\mathbf{q}_1, \mathbf{q}_2) \hat{a}^\dagger(\mathbf{q}_1) \hat{a}^\dagger(\mathbf{q}_2) |vac\rangle, \quad (5.5)$$

$$|\psi^{(2)}\rangle = \int d\mathbf{q}_1 d\mathbf{q}_2 d\mathbf{q}_3 d\mathbf{q}_4 \phi(\mathbf{q}_1, \mathbf{q}_2) \phi(\mathbf{q}_3, \mathbf{q}_4) \hat{a}^\dagger(\mathbf{q}_1) \hat{a}^\dagger(\mathbf{q}_2) \hat{a}^\dagger(\mathbf{q}_3) \hat{a}^\dagger(\mathbf{q}_4) |vac\rangle. \quad (5.6)$$

In the equation above  $\phi(\mathbf{q}_1, \mathbf{q}_2)$  is the biphoton wavefunction. The coefficients  $A, B$  and  $C$  depend on each other\*:  $C = B^2/2$  and  $A = 1 - B^2\Gamma - 12C^2\Gamma^2$ . The constant  $\Gamma = \iint d\mathbf{q}_1 d\mathbf{q}_2 |\phi(\mathbf{q}_1, \mathbf{q}_2)|^2$  accounts for the normalization of  $\phi$  and can be assumed to be one.  $B$  is proportional to the non-linear Hamiltonian and can be calculated using Eq. 5.3 and the non-linear Hamiltonian.

### 5.2.2 Orbital Angular Momentum Basis

The non-linear term can be written in the Schrödinger picture in terms of OAM modes as [17, 59]

$$\hat{H}_{NL} = \frac{1}{2} ik\hbar \sum_{\ell} \hat{a}_{\ell}^{\dagger} \hat{a}_{\ell}^{\dagger} - \hat{a}_{\ell} \hat{a}_{\ell} \quad (5.7)$$

---

\*The letters to represent the variables are chosen to match the choices of Sabharwal [40].

where  $\ell$  runs over all possible positive OAM states, we define  $\bar{\ell} \equiv -\ell$  and all constants are absorbed into  $\kappa$ . This expression is obtained by a basis transformation from the Hamiltonian in terms of linear momentum modes (Eq. 4.29).

Note that the Laguerre-Gauss modes do not form a complete basis when  $p$  is neglected. Thus this Hamiltonian cannot exactly describe the Hamiltonian in the momentum basis. From the decomposition of the PDC state it is evident that Eq. 5.7 is at least ‘well enough’: the PDC field can be described in  $\ell$ -modes thus the process generating the PDC field can be described in  $\ell$ -modes.

### Four Photon PDC State

By using this Hamiltonian in the expansion of Eq. 5.3, the first order term are all single photon states. This result was explored in detail in Sec. 4.4.3 in the momentum basis. In the OAM basis the single pair state can be written as:

$$|\psi_2\rangle = \sum_{\ell} \gamma_{\ell} |1_{\ell}; 1_{\bar{\ell}}\rangle. \quad (5.8)$$

This expression is the bi-photon wave function as a sum over modes of  $\ell$  where  $\gamma_{\ell}$  is a constant determined by the decomposition. The numbers in the ket are the number of photons in the state with subscript  $\ell$ .

The second order term produces the four-photon wave-function. The Hamiltonian is applied twice, as a result four photons will exist in the down-converted field. Expressed in a similar way [59],

$$|\psi_4\rangle = \sum_{\ell} \alpha_{\ell} |2_{\ell}; 2_{\bar{\ell}}\rangle + \frac{1}{2} \sum_{\ell_1} \sum_{\ell_2, \ell_1 \neq \ell_2} \beta_{\ell_1 \ell_2} |1_{\ell_1}, 1_{\ell_2}; 1_{\bar{\ell}_1}, 1_{\bar{\ell}_2}\rangle. \quad (5.9)$$

In the equation above the first term denotes the photon pairs emitted by stimulated emission. These pairs are in the same state. The second term are all other states, spontaneous double pairs [58]. These states are not mutually correlated [20].

### Stimulated Emission Contributions

These mutually correlated four photon states are of interest. The following argument is a lot more difficult for the general space. In a down-conversion event only the state  $\ell, \bar{\ell}$  and 0 are relevant because there are

only two allowed states for the down-converted photons:  $\ell$  and  $\bar{\ell}$  (assuming  $\ell_p = 0$  for the pump). Thus limiting the discussion to a 3 mode subspace, the PDC state is governed by

$$|\psi\rangle = \exp\left(\frac{i\hat{H}t}{\hbar}\right) |\psi_0\rangle, \quad (5.10)$$

where the Hamiltonian in the 3 mode subspace is

$$\hat{H} = i\kappa\hbar(\hat{a}_\ell^\dagger\hat{a}_{\bar{\ell}}^\dagger - \hat{a}_\ell\hat{a}_{\bar{\ell}}) + \frac{1}{2}i\kappa\hbar(\hat{a}_0^\dagger\hat{a}_0^\dagger - \hat{a}_0\hat{a}_0). \quad (5.11)$$

The extra factor of two is because the mode in  $\ell$  has two contributions since the sum is from negative infinity to positive infinity. In a sense, it can be considered looking at 2 modes because of the double contribution at  $\ell$ . Making use of the disentangling theorem [60, Eq. 5.26]

$$e^{\theta(\hat{a}_1^\dagger\hat{a}_2^\dagger - \hat{a}_1\hat{a}_2)} = e^{\Gamma\hat{a}_1^\dagger\hat{a}_2^\dagger} e^{-g(\hat{a}_1^\dagger\hat{a}_1 + \hat{a}_2^\dagger\hat{a}_2 + 1)} e^{-\Gamma\hat{a}_1\hat{a}_2} \quad (5.12)$$

where  $\Gamma = \tanh\theta$  and  $g = \ln(\cosh\theta)$ . Using the Cauchy product rule, standard properties of the creation and annihilation operators and the series definition of the exponential, the down-converted state can be written as

$$|\psi\rangle = |\psi_0\rangle + |\psi_\ell\rangle; \quad (5.13)$$

$$|\psi_0\rangle = \sum_n \frac{\tanh^n(\kappa t)}{\sqrt{\cosh(\kappa t)}} \frac{\sqrt{(2n)!}}{n!} \left(\frac{1}{2}\right)^n |2n_{\ell=0}\rangle, \quad (5.14)$$

$$|\psi_\ell\rangle = \sum_n \frac{\tanh^n(\kappa t)}{\sqrt{\cosh(\kappa t)}} |n_\ell; n_{\bar{\ell}}\rangle. \quad (5.15)$$

As argued before,  $\kappa t$  is extremely small. Taking the lowest non-zero order Taylor expansion of this expression for  $\kappa t$  near zero and truncating the sum after  $n = 2^*$ :

$$|\psi_0\rangle \approx \left(1 - \frac{(\kappa t)^2}{4}\right) |0\rangle + \frac{\kappa t}{\sqrt{2}} |1_0; 1_0\rangle + \sqrt{\frac{3}{8}}(\kappa t)^2 |2_0; 2_0\rangle \quad (5.16)$$

$$|\psi_\ell\rangle \approx \left(1 - \frac{(\kappa t)^2}{2}\right) |0\rangle + \kappa t |1_\ell; 1_{\bar{\ell}}\rangle + (\kappa t)^2 |2_\ell; 2_{\bar{\ell}}\rangle. \quad (5.17)$$

This equation explains why the down-converted state after the beamsplitters is a Dicke state [17].

---

\*It is easily shown by the ratio test that this series is convergent.

There are issues with this expression. The last term only accounts for the four-photon state due to stimulated emission. Furthermore, because we assumed  $\ell$  to be any OAM mode the state in the whole space would be the sum over all  $\ell > 0$  plus the  $\ell = 0$  state:

$$|\psi\rangle = |\psi_0\rangle + \sum_{\ell>0} |\psi_\ell\rangle. \quad (5.18)$$

Obviously this cannot be the case, the coefficients are not dependent on  $\ell$  and do not decrease as  $\ell$  increases. This would lead to an infinitely large PDC state that can not be normalized. In the decomposition of the PDC state it is observed that the coefficients decrease as  $|\ell|$  increases. To find this decomposition it is needed to find the spatial correlations first; this expression is decomposed into  $\ell$ -modes.

### 5.3 Spatial PDC Field

To find an expression for the PDC field of two photon pairs, correlation functions are calculated. The auto-correlation gives the intensity of the field. It can be calculated by

$$\langle \psi | \hat{E}^\dagger \hat{E} | \psi \rangle \quad (5.19)$$

where  $|\psi\rangle$  is the PDC state found earlier (Eq. 5.4).

The electric field operator in the paraxial approximation can be written as [40]

$$\hat{E}(\boldsymbol{\rho}, z) = \frac{1}{2\pi} e^{ikz} \int d\mathbf{q} e^{i\left(\mathbf{q}\cdot\boldsymbol{\rho} - \frac{q^2 z}{2k}\right)} \hat{a}(\mathbf{q}). \quad (5.20)$$

Eq. 5.19 with the PDC state up to second order (Eq. 5.4) can be expanded to nine terms of which only two are non-zero:

$$\langle \psi^{(1)} | \hat{E}^\dagger \hat{E} | \psi^{(1)} \rangle \quad (5.21)$$

$$\langle \psi^{(2)} | \hat{E}^\dagger \hat{E} | \psi^{(2)} \rangle \quad (5.22)$$

To calculate these terms the creation and annihilation operators must be manipulated to place them in normal order\*, this is done by using the

---

\*Normal ordering of creation and annihilation operators is placing the annihilation operators to the rightmost. When applying the operator train to the vacuum state, any annihilation operators on the right reduce the vacuums state to zero before the state can be applied to a creation operator. This simplifies the resulting expression.

commutation relation

$$[\hat{a}(\mathbf{q}), \hat{a}^\dagger(\mathbf{q}')] = \delta(\mathbf{q} - \mathbf{q}'). \quad (5.23)$$

Note that  $\hat{a}(\mathbf{q}), \hat{a}^\dagger(\mathbf{q})$  are in the space of all wave vectors in mode  $q$ , this means that  $\hat{a}(\mathbf{q})$  and  $\hat{a}(\mathbf{q}')$  work on the same space, just at a different frequency.

### One Photon Pair

For Eq. 5.21, the electric field operator applied to the state must first be calculated:

$$E \left| \psi^{(1)} \right\rangle = \frac{1}{2\pi} e^{ikz} \int d\mathbf{q} e^{i\left(\mathbf{q} \cdot \boldsymbol{\rho} - \frac{q^2 z}{2k}\right)} \hat{a}(\mathbf{q}) \iint d\mathbf{q}_1 d\mathbf{q}_2 \phi(\mathbf{q}_1, \mathbf{q}_2) \hat{a}^\dagger(\mathbf{q}_1) \hat{a}^\dagger(\mathbf{q}_2) |vac\rangle. \quad (5.24)$$

This means putting  $\hat{a}(\mathbf{q}) \hat{a}^\dagger(\mathbf{q}_1) \hat{a}^\dagger(\mathbf{q}_2)$  in normal order. Using the commutation relation this becomes

$$\hat{a}(\mathbf{q}) \hat{a}^\dagger(\mathbf{q}_1) \hat{a}^\dagger(\mathbf{q}_2) = \hat{a}^\dagger(\mathbf{q}_1) \hat{a}^\dagger(\mathbf{q}_2) \hat{a}(\mathbf{q}) + \hat{a}^\dagger(\mathbf{q}_1) \delta(\mathbf{q} - \mathbf{q}_2) + \hat{a}^\dagger(\mathbf{q}_2) \delta(\mathbf{q} - \mathbf{q}_1). \quad (5.25)$$

Applying this to the vacuum state results in an expression for  $E \left| \psi^{(1)} \right\rangle$ :

$$\frac{1}{2\pi} e^{ikz} \int d\mathbf{q} e^{i\left(\mathbf{q} \cdot \boldsymbol{\rho} - \frac{q^2 z}{2k}\right)} \left[ \int d\mathbf{q}_1 \phi(\mathbf{q}_1, \mathbf{q}) \hat{a}^\dagger(\mathbf{q}_1) + \int d\mathbf{q}_2 \phi(\mathbf{q}, \mathbf{q}_2) \hat{a}^\dagger(\mathbf{q}_2) \right] |vac\rangle. \quad (5.26)$$

Because photons are bosons,  $\phi(\mathbf{q}_1, \mathbf{q}_2) = \phi(\mathbf{q}_2, \mathbf{q}_1)$ . The integrals result in the same outcome, therefore we multiply by two and obtain

$$E \left| \psi^{(1)} \right\rangle = \frac{1}{\pi} e^{ikz} \iint d\mathbf{q} d\mathbf{q}_1 e^{i\left(\mathbf{q} \cdot \boldsymbol{\rho} - \frac{q^2 z}{2k}\right)} \phi(\mathbf{q}_1, \mathbf{q}) \hat{a}^\dagger(\mathbf{q}_1) |vac\rangle. \quad (5.27)$$

To keep the expression readable, we define

$$\Theta^I(\boldsymbol{\rho}, z, \mathbf{q}_1) = \int d\mathbf{q} e^{i\left(\mathbf{q} \cdot \boldsymbol{\rho} - \frac{q^2 z}{2k}\right)} \phi(\mathbf{q}_1, \mathbf{q}). \quad (5.28)$$

Using the expression for  $E \left| \psi^{(1)} \right\rangle$ , Eq. 5.21 can be evaluated. The conjugate of  $E \left| \psi^{(1)} \right\rangle$  results in an annihilation operator, the operators again need to be put in normal ordering using the commutation relation. This results in

an expression for the auto-correlation of the first order non-linear contribution:

$$\langle \psi^{(1)} | \hat{E}^\dagger \hat{E} | \psi^{(1)} \rangle \quad (5.29)$$

$$= \langle vac | \frac{1}{\pi^2} \iint d\mathbf{q}_1 d\mathbf{q}_2 (\Theta^I)^*(\boldsymbol{\rho}, z, \mathbf{q}_1) \Theta^I(\boldsymbol{\rho}, z, \mathbf{q}_2) \hat{a}(\mathbf{q}_1) \hat{a}^\dagger(\mathbf{q}_2) | vac \rangle \quad (5.30)$$

$$= \langle vac | \frac{1}{\pi^2} \iint d\mathbf{q}_1 d\mathbf{q}_2 (\Theta^I)^*(\boldsymbol{\rho}, z, \mathbf{q}_1) \Theta^{2D}(\boldsymbol{\rho}, z, \mathbf{q}_2) \times [\hat{a}^\dagger(\mathbf{q}_2) \hat{a}(\mathbf{q}_1) + \delta(\mathbf{q}_2 - \mathbf{q}_1)] | vac \rangle \quad (5.31)$$

$$= \frac{1}{\pi^2} \int d\mathbf{q}_1 |\Theta^I(\boldsymbol{\rho}, z, \mathbf{q}_1)|^2. \quad (5.32)$$

This is what is intuitively expected. The expression above is the square of the modulus of the Fourier transform of the biphoton wavefunction, where one coordinate is integrated over. This traces out one quasi-probability distribution and leaves the probability to find a photon at a point, essentially the integral over all momenta for the other photon. For two photon pairs this becomes significantly more complex.

### Two Photon Pairs

For two photon pairs the procedure is applied to the second order term of the PDC state. The normal ordering gets a lot more tedious but applying the commutation relation is still straightforward. A method for working out the expression is by using Wick's theorem, presented in Appx. A.1. The result is

$$\begin{aligned} \langle \psi^{(2)} | \hat{E}^\dagger \hat{E} | \psi^{(2)} \rangle &= \frac{8}{\pi^2} \left[ \Gamma \int d\mathbf{q}_3 |\Theta^I(\mathbf{q}_3)|^2 \right. \\ &\quad \left. + 2 \int d\mathbf{q}_1 \int d\mathbf{q}_3 (\Theta^I(\mathbf{q}_3))^* \phi(\mathbf{q}_1, \mathbf{q}_3) \int d\mathbf{q}_2 \Theta^I(\mathbf{q}_2) \phi^*(\mathbf{q}_1, \mathbf{q}_2) \right]. \end{aligned} \quad (5.33)$$

The first term is responsible for independent photon pairs while the second term describes the entangled pairs. The integral is over both bi-photon wave functions, it is not separable. By definition it is entangled.

The equation above agrees exactly with the results in Sabharwal's thesis [40, Ch 2.7] if the beamsplitter is ignored. The equation for a single photon pair (Eq. 5.32) is off by a factor of two when compared to Sabharwal's result.

# Experimental Setup

The optical setup, as drawn in Fig. 6.1 and described in Sec 6.1, is controlled via a computer using spatial light modulators (SLMs). The light is collected by fibers which are coupled to single photon counters. These counters are connected to a time-tagging card and coincidences are counted using software; these counts are key to demonstrating entanglement.

## 6.1 Optics

The pump beam is generated by a mode-locked Ti:Sapphire laser which sends out pulses of roughly 2 ps length at a power of 2 W. This light is up-converted in a sum frequency generation (SFG) module resulting in a power of 150 mW at 413 nm on the table. The beam passes through a waveplate to match the polarization to that of the PPKTP crystal. A 250 mm focusing lens is used to focus the beam in the crystal after which a 413 nm filter blocks any fluorescence from previous optical components along with any residual 826 nm light. The beam is focused into the periodically poled non-linear crystal, held at a constant temperature of 62°C, along its optical axis. Upon exiting the crystal a gallium phosphide plate is placed to attenuate the pump beam severely\*. The beam is collimated again by a 40 mm lens after which it passes through a narrow-band filter centered around 826 nm with a width of 10 nm. This filter removes non-phase matched photons from the spectrum of SPDC light to strengthen the relative intensity of entangled photons and thus reduce error. A polarizer is used to remove unwanted modes of light. A 750 mm lens makes an im-

---

\*The needed attenuation is at least  $10^{-10}$ , this number is calculated from the ratio of incident light on the crystal and down-converted light emitted.

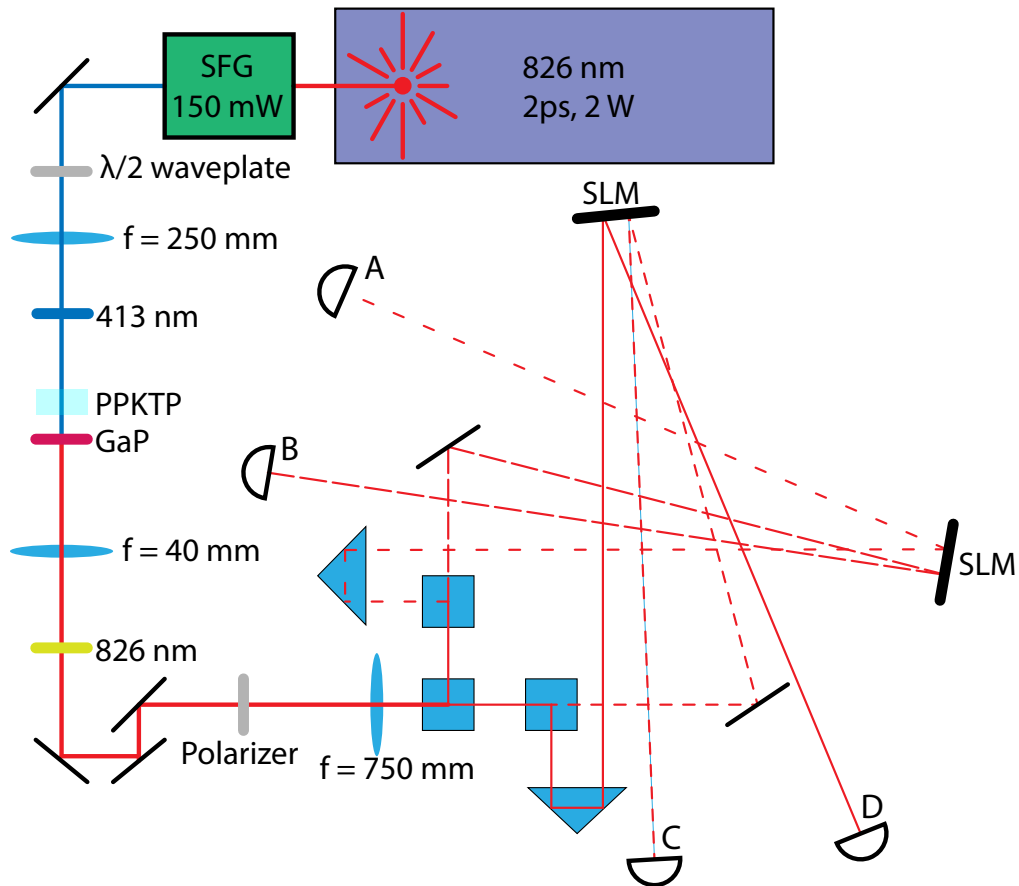


**Figure 6.1:** Schematic drawing of the experimental set-up. A Ti:Sapphire laser emits 2 W of laser light at a wavelength  $\lambda = 826$  nm with a pulse length of 2 ps. This passes through a sum-frequency generation crystal which outputs 150 mW at half the wavelength. The bundle encounters a  $\lambda/2$  waveplate, a focussing lens and a filter that blocks the infrared light before passing through a PPKTP crystal. Behind this crystal is a galium phosphide plate acting as a filter that blocks the light at 413 nm. The bundle is collimated by a lens and encounters a 10 nm narrowband filter at 826 nm. After some mirrors, a polarizer lets only the desired H-polarized PDC photons through. A lens makes an image onto the SLMs, which the bundle hits after being split into four by three beamsplitters. Each beam, A, B, C and D, are coupled to a fiber ending at a single photon detector. The signals from the single photon detectors are processed further digitally to count coincidences.

age onto the SLMs, between those two components the beam is split into four. This is done by two successive beamsplitters resulting in beams A, B, C and D. Beams A and D encounter a retro-reflector before hitting the SLM; beams B and C a mirror. The retro-reflectors allow adjusting the path length by simply translating them along the direction of the beam. Upon reflection by the SLM each beam is coupled to a single-mode fiber heading into a single photon detector.

## 6.2 SLMs

Spatial light modulators are used to post-select the OAM mode of the beams coming out of the crystal. They are driven by a computer displaying holographic images on them. These holograms are designed to change the OAM and other properties of the beam by creating fork holograms and applying Zernike polynomials to them. In reality this does not post-select for Laguerre-Gauss modes but for Kummer beams [61]. The difference is not very large and the theory developed for Laguerre-Gauss modes is a good approximation.

## 6.3 Coincidence counts

If two photons hit the detector within a predetermined time, they are determined to be temporally correlated and it is most likely that they originate from the same laser pulse. These two photons are probably a pair, or part of two photon pairs. The coincidence counts are determined by time-tagging all incoming photons and grouping photons that arrive within a certain time.

## 6.4 Anti-Correlation of Orbital Angular Momentum

The angular momentum is measured by taking two beams, say A and B, and varying the images on the SLMs in such a way that a Laguerre-Gauss mode in  $(\ell_A, p_A) = (i, 0)$  and  $(\ell_B, p_B) = (j, 0)$  is shifted to the  $(0, 0)$  mode. The resulting beam is captured by the fiber; a projection of only the desired mode. This projection is the post selection of the OAM mode. The counter  $i \in [-\ell_{\max}, \ell_{\max}]$  is going through all its values for every value of  $j \in [-\ell_{\max}, \ell_{\max}]$ . For all pairs  $i, j$  the coincidence counts are measured. These

are then plotted with the OAM of a detector on an axis; an anti-diagonal line is expected if the photons are indeed entangled.

## Results

Measurements were made using the set-up as described in Ch. 6. First, experimental evidence for the conservation of OAM is presented. After establishing the conservation of OAM, the measurements of power dependent counts are presented.

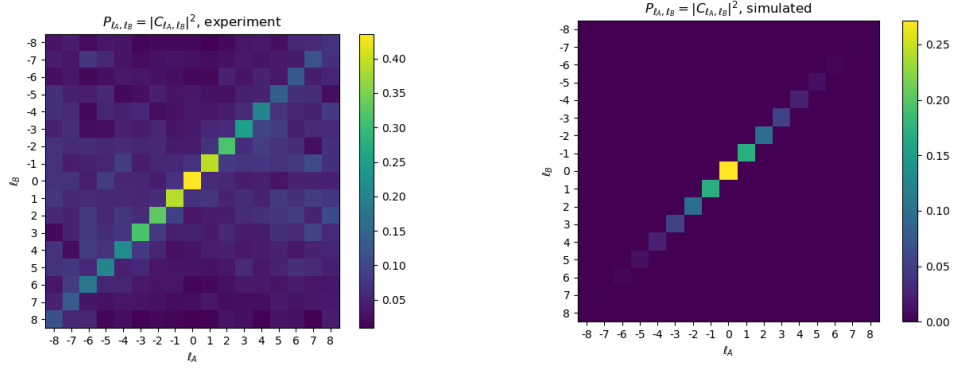
### 7.1 Conservation of Orbital Angular Momentum

The OAM was measured using the procedure outlined in Sec. 6.4; the PDC light was split using a beamsplitter and OAM mode  $\ell$  was projected onto a single mode fiber by an SLM. Measured counts for combinations of  $\ell$ -modes are shown in Fig. 7.1a. The same experiment was done numerically by calculating the coefficients in Eq. 4.63, the results of which are shown in Fig. 7.1b. The experimental data shows that the detection of photon pairs in an OAM mode is anti-correlated; the detection probability is highest when  $\ell_A = -\ell_B$ .

Results from the simulation agree well with the experiment, making an argument that the measurement can be explained by the theory in Sec. 4.5.4. As argued in Sec. 4.5.4, OAM is a conserved quantity. The measured data supports this result.

### 7.2 Power Dependent Counts

The single photon counts were measured at two detectors as a function of pump beam power. The difference in counts between the two detectors was not very large as can be seen in Fig. 7.2. This figure also implies that one detector is more efficient near  $\ell = 0$ , for higher  $|\ell|$  the other detector



(a) Experimental results.

(b) Simulated results.

**Figure 7.1:** Decomposition of the down-converted field created by a Gaussian ( $\ell = 0$ ) pump beam. Both figures use a logarithmic scale. The left figure (Fig. 7.1a) shows experimental results, the right figure (Fig. 7.1b) shows simulated results of the same experiment. On the horizontal axis is the  $\ell$ -mode detected by one detector, on the vertical axis is the  $\ell$ -mode detected by the other detector. Both figures show anti-correlations in their  $\ell$ -modes by a distinct trace along the anti-diagonal.

performs better. To declutter the data, the mean counts of the two detectors is taken. This mean is what is meant when referred to ‘single counts’ and what is plotted for different  $\ell$ -modes in Fig. 7.3a. In Fig. 7.3b the coincidence counts are plotted, these are the photon pairs arriving at both detectors within a small time interval.

In the obtained data there appears to be a linear relation in the single counts and a second order polynomial can be used to describe the coincidence counts. This relation is probably due to the fact that there is a chance to detect a photon  $P_{\text{detect}}$  for each detector. The assumption is that all light minus the dark counts which hit the detector is PDC light, every count is a photon which depends linearly on the pump power. The coincidence counts are these photons, however they are temporally correlated. Both photons need to detect a photon within a time interval, therefore the correlation counts should go with the square of the detection probability.

### 7.2.1 Single Counts

The single counts arriving at the detector correspond directly to the intensity of the PDC field. Part of this will be the higher order interactions, these contributions are negligible compared to the single counts. From the dependence of the non-linear Hamiltonian on the pump power as in

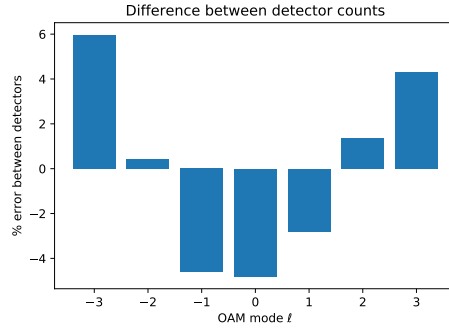


**Figure 7.2:** The relative error in detection rate between the two detectors used. On the horizontal axis is the OAM mode  $l$  from -3 to 3. The vertical axis displays the relative error between the single counts of the detectors in percentages. The calculation was performed with the data corrected for dark counts. The shape of the figure implies that one detector detects modes near the fundamental better compared to the other; the error is in one detector's favor near  $l = 0$  and at high  $|\ell|$  the other detector performs better.

Eq. 4.44, it is expected that the single counts scale linearly with the pump power. The obtained single counts are plotted in Fig. 7.3a. The data is corrected for dark counts and a power offset. The corrected data is fitted to a linear relation for each measured  $l$ -mode.

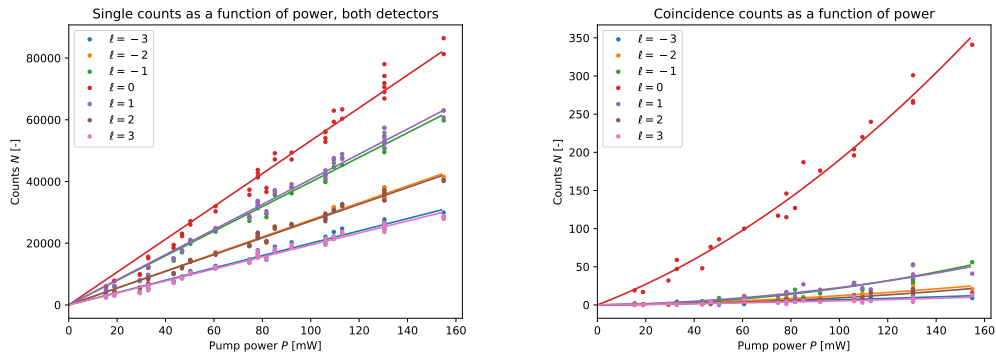
Using the slope of the fit as a measure for interaction strength in an  $l$ -mode, the contributions of the measured modes can be plotted relative to each other. A bar graph of the contributions for the various modes is plotted in Fig. 7.4a.

The linear relation in the single photon counts (Fig. 7.3a) are suspected to be due to the single photon pairs. The theory predicts that single pair intensity goes linearly with the pump power, the experiment confirms that relation. In Fig. 7.4a the coefficient of the linear dependence is shown. This is interpreted to be the OAM spectrum of the PDC light. Comparing this to Fig. 7.1 the behavior looks the same, there is a maximum at  $l = 0$  and the intensity decreases as  $|\ell|$  grows.

## 7.2.2 Coincidence Counts

Fig. 7.3b shows the coincidence counts as function of the pump power. It is expected that these counts contain mostly two photon contributions. The data corrected for systematic errors was fitted to

$$N_{CC} = ax^2 + bx. \quad (7.1)$$



(a) Mean of the single counts as measured by the detectors. The data is fitted to a linear relation. (b) Coincidence counts between the detectors. The data is fitted to a quadratic relation.

**Figure 7.3:** In the left figure (Fig. 7.3a) the relationship between the detector counts corrected for the dark counts is plotted against the pump laser power. It shows a linear relation. The right figure (Fig. 7.3b) shows the same relation for the coincidence counts; photons hitting the two detectors at the same time (within a small time delay). The coincidence counts appear to go quadratic with the laser power.

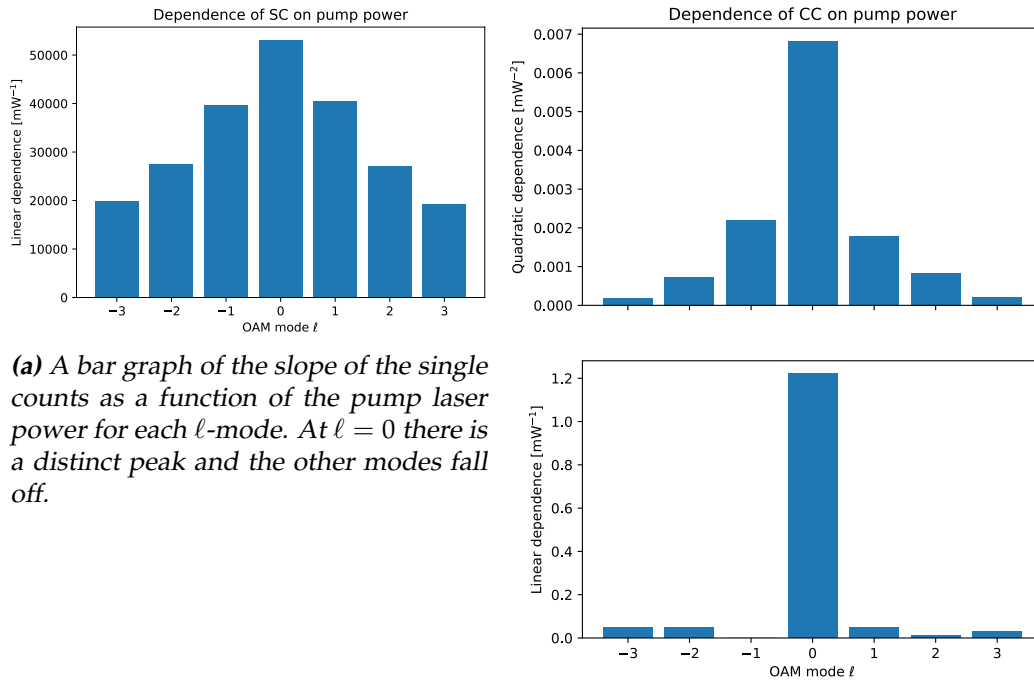
Fig. 7.4b shows the slope of this fit for each  $\ell$ -mode. The fit parameter for the quadratic part decreases as  $|\ell|$  increases. The linear fit parameter is large for  $\ell = 0$  and nearly zero for other  $\ell$ .

In Fig. 7.3b there is not a linear relation in the experimental data. It is suspected that a second degree polynomial will make a satisfying fit. In both polynomials the constant coefficient is set to zero as the data is already corrected for dark counts. The quadratic term is due to the probability of detecting two photons from the same pair being the square of the single detection probability.

Fig. 7.4b shows the relative strength of the coefficients in the polynomial. The  $\ell = 0$  mode contains a definite linear dependence. This linear dependence can be caused by non phase-matched fluorescence; these photons are from the same pulse and will thus register as a coincidence count.

## 7.3 Numerical Experiments

In order to calculate the decomposition of the PDC field the correlation function must be calculated first. A partial expression was derived for the four photon correlation function in Appx. A. To explore if the four photon



(a) A bar graph of the slope of the single counts as a function of the pump laser power for each  $\ell$ -mode. At  $\ell = 0$  there is a distinct peak and the other modes fall off.

(b) The upper figure is a bar graph of the quadratic contributions to the coincidence counts as a function of the pump laser power for each  $\ell$ -mode. The lower figure shows the linear contributions in the same fashion.

**Figure 7.4:** All sub-figures show the dependence of a fit parameter depending on the OAM mode of the light. The left figure (Fig. 7.4a) shows the strength of the linear dependence from the fits in Fig. 7.3a. In the figure on the right (Fig. 7.4b) the strength of the dependence on the quadratic and linear term are shown.

correlation function behaves like is expected numerical experiments were run, this turned out not to account for all pairs.

The spatial correlation function for two photons as derived and calculated in Sabharwal's thesis was reproduced [40]. This results in Fig. 7.5. From the comparison it was discovered that the derived expression is incomplete, for this reason it is left in the appendix.

### 7.3.1 Spatial Correlations

A direct approach is described by Sabharwal, the two detector correlation function from [40] was repeated by simulation (Fig. 7.5). Fig. 7.5a shows independent counts in the simulation. This is the product of the field at

each detector,

$$G^{(ind)}(x_1, x_2, z) = \langle \psi | \hat{E}^\dagger(x_1) \hat{E}(x_1) | \psi \rangle \langle \psi | \hat{E}^\dagger(x_2) \hat{E}(x_2) | \psi \rangle. \quad (7.2)$$

These counts are needed as a correction to determine the entangled double pair correlations.

In Fig. 7.5b there are lines visible along the diagonal and anti-diagonal. There is also a plus shape centered around  $(0, 0)$ .

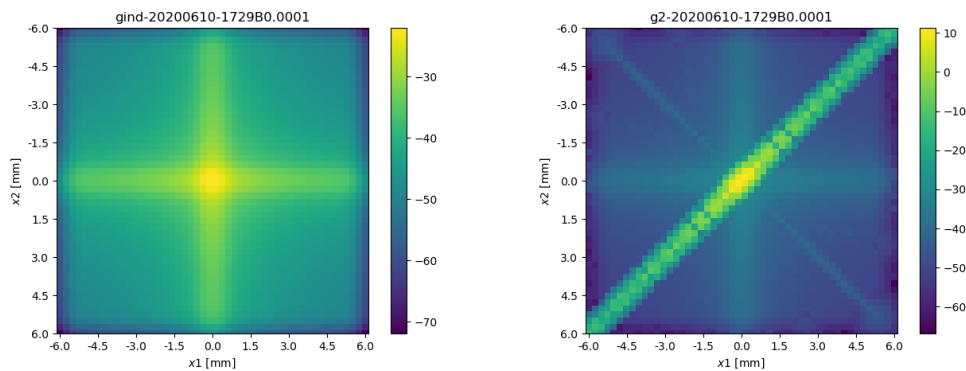
By subtracting the independent counts from the correlations the dependent counts are obtained. These 'true' correlations are the single and double entangled photon pairs.

In Fig. 7.5b, there are strong anti-diagonal correlations are visible. These correlations imply a single photon pair. This pair can either be on its own or part of a double pair. The off-diagonal shows some fringes, this is a result of the sinc-shaped phase matching function.

On the diagonal there are weaker correlations, these imply four entangled photons. This can be from spontaneous double pairs or two independent pairs which happen to be in the same state, in either case the line along the diagonal implies two entangled pairs.

There is a plus shape visible centered at  $(0, 0)$ . This is due to the way the field is structured, the intensity is high near zero. Finding a photon at a position  $x \neq 0$  while the other detector is near zero does not say a lot about correlations because there are lots of photons there; the detectors will click simultaneously 'by accident'.

These results agree with Sabahrwal's results. These simulations used different parameters; the images do not look identical to the one in Sabahrwal's thesis. Qualitatively the simulation agrees and contains all main results: spatial correlations and evidence of stimulated pairs.



**(a)** Independent counts in the spatial correlations. This is the overlap of the field at both detectors. The figure shows a plus along the main axes.

**(b)** Spatial correlations between two detectors at  $x_1$  and  $x_2$  at different output ports of a beamsplitter. A strong anti-correlation can be seen along the anti-diagonal. Weaker correlations can be seen along the diagonal. There are also correlations when either coordinate is zero, resulting in a plus shape.

**Figure 7.5:** Independent and correlated photon counts from a simulation. Both figures make use of a logarithmic scale for the intensity.



## Discussion

The results as presented in Ch. 7 can be interpreted as evidence for the conservation of OAM and further confirmation for the SPDC theory as outlined in Ch. 4. In this chapter, potential sources of errors will be considered as well as future avenues to explore.

### 8.1 Conservation of Orbital Angular Momentum

Figures like Fig. 7.1a have been obtained for all pairs of detectors in the experimental setup. Due to problems with equipment and time constraints four-photon correlations were not measured successfully. It would be of value to make such a measurement and compare it to the theory from Sec. A.2.

The results from Sec. 7.3.1 involve the PDC far field. This is however not useful to the experiment as the crystal is imaged onto the SLMs; in principle no Fourier transform is needed. However, this does not matter since zero modes are propagation invariant (the Fourier transform of a Gaussian is again a Gaussian), in this setup the numerical aperture is low and finally after the SLM the field is propagated to fibers in the far field.

### 8.2 Power Dependent Counts

The setup most likely contains double photon pairs. Double pairs could be detected: when detecting two photons in the same mode, these would be two photons from the entangled pairs. In the gathered data the counts are too little to detect double pairs. With more careful alignment and a longer integration time this is perhaps possible.

### 8.3 Four Photon Correlation Function

In Appx. A steps are set towards a four photon correlation function. This is a work in progress. There is discussion about the best route towards describing these higher order interactions. One point to consider is that the derivation of the PDC process arbitrarily truncates the Taylor expansion of the electric susceptibility at the second order; processes such as three wave mixing are completely ignored. Another concern is that the approximation of the down-converted state is also truncated and has to be normalized again for every extra term taken into account.

### 8.4 Reflecting on the Experiment

In the setup as outlined in Ch. 6, there have been some problems with the equipment used which should be addressed.

The set-up contains various optical elements in which fluorescence can be an issue. Examples are the lenses, beamsplitters, filters and retro-reflectors. Although the optical elements are chosen in such a way to minimize fluorescence and a narrowband filter is placed in the down-converted beam, it is not guaranteed that there is absolutely no fluorescence.

During the experiment there have been instability issues with the Spectra-Physics Tsunami laser. After a while the laser stopped pulsing, thereby making the beam on the optical table continuous wave and greatly reducing the intensity of the beam. It turned out that this was due to a broken cooler. Over short periods of time the laser appears stable, this issue has not impacted the measurements presented in Ch. 7.

The 826 nm narrow band filter in Fig. 6.1 was deteriorated to a barely usable point. By rotating the filter a spot could be found that produced acceptable counts. To reduce effects of the broken filter it was placed in the near field to minimize its effects on the far field profile of the beam. This filter should be replaced by a new one.

One SLM was showing signs of deterioration. The lens that focused the beam in the crystal was later replaced by a stronger lens in an attempt to increase the power density inside the crystal. This is supposed to lead to more PDC pair production.

Still, the optical setup is an extremely accurate device delivering impressive capabilities. There is much more to explore with it such as successfully measuring four photon OAM coefficients and comparing it to the theory, confirming entanglement by measuring in different bases, taking another look at the second pair production at different laser powers and

determining the ratio between the first and second pair production rate or  
determining the ratio of spontaneous and stimulated pair production.



# Towards the Derivation of a Fourth Order Correlation Function

A lot of effort has been directed towards calculating the four detector correlation function. After a failed attempt where terms were missing another attempt was made that violates energy conservation. This last attempt rests on Wick's theorem, explained below.

## A.1 Wick's Theorem

We define  $:\hat{O}:$  as the normal ordering of the  $\hat{O}$  operator. Let the contraction be defined as

$$\hat{A}\hat{B} \equiv \hat{A}\hat{B} - :\hat{A}\hat{B}: \quad (\text{A.1})$$

Note that for the commutation relation  $[\hat{a}(q_i), \hat{a}^\dagger(q_j)] = \delta(q_i - q_j)$  the following relations are trivially seen to be (for simplicity of notation let  $\hat{a}_i \equiv \hat{a}(q_i)$ ):

$$\hat{a}_i \hat{a}_j = 0 \quad (\text{A.2})$$

$$\hat{a}_i^\dagger \hat{a}_j^\dagger = 0 \quad (\text{A.3})$$

$$\hat{a}_i^\dagger \hat{a}_j = 0 \quad (\text{A.4})$$

$$\hat{a}_i \hat{a}_j^\dagger = \delta_{ij} \quad (\text{A.5})$$

These contraction relations simplify the application of Wick's theorem.

Wick's theorem can be stated as

$$\begin{aligned}
\hat{A}\hat{B}\hat{C}\hat{D}\hat{E}\dots &=: \hat{A}\hat{B}\hat{C}\hat{D}\hat{E}\dots : \\
&+ \sum_{\text{singles}} : \hat{A}\bullet\hat{B}\bullet\hat{C}\hat{D}\hat{E}\dots : \\
&+ \sum_{\text{doubles}} : \hat{A}\bullet\hat{B}\bullet\bullet\hat{C}\bullet\bullet\hat{D}\bullet\hat{E}\dots : \\
&+ \dots
\end{aligned} \tag{A.6}$$

Repeated bullets differentiate between different contractions. Wick's theorem enjoys multiple applications in QFT, we will be using it to calculate the correlation function. Since we will be applying this to a vacuum state all terms containing normal ordered operators reduce to zero. The only surviving terms will be those where all operators are contracted. In practice, this means that the operators are reduced to a sum of delta functions containing all permutations of the indices. Armed with Wick's theorem an attempt at four detector correlations is made.

## A.2 Four Detector Correlations

How is it possible to determine entanglement of four photons? To start, they should be temporally and spatially correlated. Below an attempt is made to derive the four detectors spatial correlation function for the PDC field. The results derived below are in no way complete and should be looked at critically. This fourth order correlation function shows spatial correlations between photons which can then be used to decompose the field into OAM modes by the procedure as shown for two photons in Sec. 4.5.3.

The fourth order correlation function is

$$G^{(4)}(\mathbf{r}_1\mathbf{r}_2\mathbf{r}_3\mathbf{r}_4) = \langle \psi | \hat{E}(\mathbf{r}_1)\hat{E}(\mathbf{r}_2)\hat{E}(\mathbf{r}_3)\hat{E}(\mathbf{r}_4)\hat{E}^\dagger(\mathbf{r}_4)\hat{E}^\dagger(\mathbf{r}_3)\hat{E}^\dagger(\mathbf{r}_2)\hat{E}^\dagger(\mathbf{r}_1) | \psi \rangle. \tag{A.7}$$

The notation  $\mathbf{r}$  signifies the dependence on  $\boldsymbol{\rho}, z$  in cylindrical coordinates while condensing the notation.

The real space biphoton wavefunction is  $\Theta^{II}$ , which can be written as

$$\Theta^{II}(\boldsymbol{\rho}_1, \boldsymbol{\rho}_2) = \langle vac | \hat{E}(\boldsymbol{\rho}_1)\hat{E}(\boldsymbol{\rho}_2) | \psi^{(1)} \rangle. \tag{A.8}$$

Since an analytic expression is known (Eq. 4.56), the four photon field can be computed without numerically evaluating integrals, significantly

speeding up computation time when compared to lower order correlation functions where integration is necessary.

The electric field operator\* in the paraxial regime is given by Eq. 5.20 and can be used to define  $\zeta$  to be

$$\hat{E}(\boldsymbol{\rho}, z) = \int d\mathbf{q} \zeta(\mathbf{q}, \mathbf{r}) \hat{a}(\mathbf{q}). \quad (\text{A.9})$$

We define the function

$$\Theta^{2D}(\mathbf{r}, \mathbf{q}_1) = \int d\mathbf{q} \zeta(\mathbf{q}, \mathbf{r}) \phi(\mathbf{q}_1, \mathbf{q}). \quad (\text{A.10})$$

We are looking for

$$\langle \Psi | \hat{E}^\dagger(\mathbf{r}_1) \hat{E}^\dagger(\mathbf{r}_2) \hat{E}^\dagger(\mathbf{r}_3) \hat{E}^\dagger(\mathbf{r}_4) \hat{E}(\mathbf{r}_4) \hat{E}(\mathbf{r}_3) \hat{E}(\mathbf{r}_2) \hat{E}(\mathbf{r}_1) | \Psi \rangle \quad (\text{A.11})$$

which can be broken down to the sum of the terms

$$\langle \psi^{(1)} | \hat{E}^\dagger(\mathbf{r}_1) \hat{E}^\dagger(\mathbf{r}_2) \hat{E}^\dagger(\mathbf{r}_3) \hat{E}^\dagger(\mathbf{r}_4) \hat{E}(\mathbf{r}_4) \hat{E}(\mathbf{r}_3) \hat{E}(\mathbf{r}_2) \hat{E}(\mathbf{r}_1) | \psi^{(1)} \rangle \quad (\text{A.12})$$

$$\langle \psi^{(2)} | \hat{E}^\dagger(\mathbf{r}_1) \hat{E}^\dagger(\mathbf{r}_2) \hat{E}^\dagger(\mathbf{r}_3) \hat{E}^\dagger(\mathbf{r}_4) \hat{E}(\mathbf{r}_4) \hat{E}(\mathbf{r}_3) \hat{E}(\mathbf{r}_2) \hat{E}(\mathbf{r}_1) | \psi^{(1)} \rangle \quad (\text{A.13})$$

$$\langle \psi^{(2)} | \hat{E}^\dagger(\mathbf{r}_1) \hat{E}^\dagger(\mathbf{r}_2) \hat{E}^\dagger(\mathbf{r}_3) \hat{E}^\dagger(\mathbf{r}_4) \hat{E}(\mathbf{r}_4) \hat{E}(\mathbf{r}_3) \hat{E}(\mathbf{r}_2) \hat{E}(\mathbf{r}_1) | \psi^{(2)} \rangle \quad (\text{A.14})$$

where

$$|\psi^{(1)}\rangle = \iint d\mathbf{q}_1 d\mathbf{q}_2 \phi(\mathbf{q}_1, \mathbf{q}_2) \hat{a}^\dagger(\mathbf{q}_1) \hat{a}^\dagger(\mathbf{q}_2) |vac\rangle, \quad (\text{A.15})$$

$$|\psi^{(2)}\rangle = \int d\mathbf{q}_1 d\mathbf{q}_2 d\mathbf{q}_3 d\mathbf{q}_4 \phi(\mathbf{q}_1, \mathbf{q}_2) \phi(\mathbf{q}_3, \mathbf{q}_4) \hat{a}^\dagger(\mathbf{q}_1) \hat{a}^\dagger(\mathbf{q}_2) \hat{a}^\dagger(\mathbf{q}_3) \hat{a}^\dagger(\mathbf{q}_4) |vac\rangle. \quad (\text{A.16})$$

It is also useful to show that

$$\int d\mathbf{q} \zeta(\mathbf{q}, \mathbf{r}) \zeta^*(\mathbf{q}, \mathbf{r}') \quad (\text{A.17})$$

$$= \int d\mathbf{q} \frac{1}{2\pi} e^{ikz} e^{i\left(\mathbf{q}\cdot\rho - \frac{q^2 z}{2k}\right)} \frac{1}{2\pi} e^{ikz'} e^{i\left(\mathbf{q}\cdot\rho' - \frac{q^2 z'}{2k}\right)} \quad (\text{A.18})$$

$$= \frac{1}{4\pi^2} e^{ik(z-z')} \int d\mathbf{q} e^{i\left(\frac{q^2(z-z')}{2k}\right)} e^{i(\mathbf{q}\cdot(\rho-\rho'))} \quad (\text{A.19})$$

---

\*It is possible to account for dispersion when calculating the spatial correlation function, dispersion adds a term to the electric field operator making it time dependent. The method is the same, the result contains an extra time dependent exponential factor in the definition of the spatial bi-photon wave function [40].

which is used to define

$$\Delta(\mathbf{r}) \equiv \frac{1}{4\pi^2} e^{ikz} \int d\mathbf{q} e^{\left(\frac{q_z^2}{2k}\right)} e^{i(\mathbf{q}\cdot\boldsymbol{\rho})} \quad (\text{A.20})$$

such that

$$\int d\mathbf{q} \zeta(\mathbf{q}, \mathbf{r}) \zeta^*(\mathbf{q}, \mathbf{r}') = \Delta(\mathbf{r} - \mathbf{r}'). \quad (\text{A.21})$$

Eq. A.13 is zero since the operators in the state can be seen as the same of A.12 with two extra annihilation operators in front. The resulting terms will always leave an annihilation operator after applying Wick's theorem, therefore the state will always be zero. We only need to work out Eqs. A.12 and A.14.

## A.2.1 Single Pair Contributions

Equation A.12 can be written as an integral:

$$\begin{aligned} & \langle \psi^{(1)} | \hat{E}^\dagger(\mathbf{r}_1) \hat{E}^\dagger(\mathbf{r}_2) \hat{E}^\dagger(\mathbf{r}_3) \hat{E}^\dagger(\mathbf{r}_4) \hat{E}(\mathbf{r}_4) \hat{E}(\mathbf{r}_3) \hat{E}(\mathbf{r}_2) \hat{E}(\mathbf{r}_1) | \psi^{(1)} \rangle \quad (\text{A.22}) \\ &= \langle vac | \int d\mathbf{q}_1 d\mathbf{q}_2 \phi^*(\mathbf{q}_1, \mathbf{q}_2) \hat{a}(\mathbf{q}_1) \hat{a}(\mathbf{q}_2) \\ & \times \int d\mathbf{q}'_1 d\mathbf{q}'_2 d\mathbf{q}'_3 d\mathbf{q}'_4 \zeta^*(\mathbf{q}'_1, \mathbf{r}_1) \zeta^*(\mathbf{q}'_2, \mathbf{r}_2) \zeta^*(\mathbf{q}'_3, \mathbf{r}_3) \zeta^*(\mathbf{q}'_4, \mathbf{r}_4) \hat{a}^\dagger(\mathbf{q}'_1) \hat{a}^\dagger(\mathbf{q}'_2) \hat{a}^\dagger(\mathbf{q}'_3) \hat{a}^\dagger(\mathbf{q}'_4) \\ & \times \int d\mathbf{q}_3 d\mathbf{q}_4 d\mathbf{q}_5 d\mathbf{q}_6 \zeta(\mathbf{q}_3, \mathbf{r}_1) \zeta(\mathbf{q}_4, \mathbf{r}_2) \zeta(\mathbf{q}_5, \mathbf{r}_3) \zeta(\mathbf{q}_6, \mathbf{r}_4) \hat{a}(\mathbf{q}_3) \hat{a}(\mathbf{q}_4) \hat{a}(\mathbf{q}_5) \hat{a}(\mathbf{q}_6) \\ & \times \int d\mathbf{q}'_5 d\mathbf{q}'_6 \phi(\mathbf{q}'_5, \mathbf{q}'_6) \hat{a}^\dagger(\mathbf{q}'_5) \hat{a}^\dagger(\mathbf{q}'_6) | vac \rangle. \quad (\text{A.23}) \end{aligned}$$

The order of integration may change, the order of the operators needs to be put into normal ordering. This sequence of operators is

$$\hat{O} \equiv \hat{a}(\mathbf{q}_1) \hat{a}(\mathbf{q}_2) \hat{a}^\dagger(\mathbf{q}'_1) \hat{a}^\dagger(\mathbf{q}'_2) \hat{a}^\dagger(\mathbf{q}'_3) \hat{a}^\dagger(\mathbf{q}'_4) \hat{a}(\mathbf{q}_1'') \hat{a}(\mathbf{q}_2'') \hat{a}(\mathbf{q}_3'') \hat{a}(\mathbf{q}_4'') \hat{a}^\dagger(\mathbf{q}'''_1) \hat{a}^\dagger(\mathbf{q}'''_2). \quad (\text{A.24})$$

Since there are as much creation as annihilation operators, Wick's theorem can be applied. We are looking at every permutation of one set of momenta while keeping the other set of momenta constant. Thus, In the last sum there will be 6! terms since one index is chosen, then there are five options for the next index, four options for the next index and so forth.

$$\delta(\mathbf{q}_1 - \mathbf{q}'_1) \delta(\mathbf{q}_2 - \mathbf{q}'_2) \delta(\mathbf{q}_1'' - \mathbf{q}'_3) \delta(\mathbf{q}_2'' - \mathbf{q}'_4) \delta(\mathbf{q}_3'' - \mathbf{q}'''_1) \delta(\mathbf{q}_4'' - \mathbf{q}'''_2) \quad (\text{A.25})$$

To clean up the notation, this is re-indexed to\*

$$\delta(\mathbf{q}_1 - \mathbf{q}'_1)\delta(\mathbf{q}_2 - \mathbf{q}'_2)\delta(\mathbf{q}_3 - \mathbf{q}'_3)\delta(\mathbf{q}_4 - \mathbf{q}'_4)\delta(\mathbf{q}_5 - \mathbf{q}'_5)\delta(\mathbf{q}_6 - \mathbf{q}'_6) \quad (\text{A.26})$$

We get the sum of terms of all permutations  $\sigma_i$  of the index of the primed coordinate:

$$\hat{\mathcal{O}} = \sum_{i=1}^{6!} \prod_{j=1}^6 \delta(\mathbf{q}_j - \mathbf{q}'_{\sigma_i(j)}) + \text{terms with operators.} \quad (\text{A.27})$$

This operator is placed in the integral

$$\begin{aligned} &= \langle vac | \int d\mathbf{q}_1 d\mathbf{q}_2 \phi^*(\mathbf{q}_1, \mathbf{q}_2) \\ &\quad \times \int d\mathbf{q}'_1 d\mathbf{q}'_2 d\mathbf{q}'_3 d\mathbf{q}'_4 \zeta^*(\mathbf{q}'_1, \mathbf{r}_1) \zeta^*(\mathbf{q}'_2, \mathbf{r}_2) \zeta^*(\mathbf{q}'_3, \mathbf{r}_3) \zeta^*(\mathbf{q}'_4, \mathbf{r}_4) \\ &\quad \times \int d\mathbf{q}_3 d\mathbf{q}_4 d\mathbf{q}_5 d\mathbf{q}_6 \zeta(\mathbf{q}_3, \mathbf{r}_1) \zeta(\mathbf{q}_4, \mathbf{r}_2) \zeta(\mathbf{q}_5, \mathbf{r}_3) \zeta(\mathbf{q}_6, \mathbf{r}_4) \\ &\quad \times \int d\mathbf{q}'_5 d\mathbf{q}'_6 \phi(\mathbf{q}'_5, \mathbf{q}'_6) \hat{\mathcal{O}} | vac \rangle \end{aligned} \quad (\text{A.28})$$

$$\begin{aligned} &= \int d\mathbf{q}_1 d\mathbf{q}_2 d\mathbf{q}_3 d\mathbf{q}_4 d\mathbf{q}_5 d\mathbf{q}_6 \int d\mathbf{q}'_1 d\mathbf{q}'_2 d\mathbf{q}'_3 d\mathbf{q}'_4 d\mathbf{q}'_5 d\mathbf{q}'_6 \\ &\quad \times \zeta^*(\mathbf{q}'_1, \mathbf{r}_1) \zeta^*(\mathbf{q}'_2, \mathbf{r}_2) \zeta^*(\mathbf{q}'_3, \mathbf{r}_3) \zeta^*(\mathbf{q}'_4, \mathbf{r}_4) \zeta(\mathbf{q}_3, \mathbf{r}_1) \zeta(\mathbf{q}_4, \mathbf{r}_2) \zeta(\mathbf{q}_5, \mathbf{r}_3) \zeta(\mathbf{q}_6, \mathbf{r}_4) \\ &\quad \times \phi^*(\mathbf{q}_1, \mathbf{q}_2) \phi(\mathbf{q}'_5, \mathbf{q}'_6) \sum_{i=1}^{6!} \prod_{j=1}^6 \delta(\mathbf{q}_j - \mathbf{q}'_{\sigma_i(j)}) \end{aligned} \quad (\text{A.29})$$

$$\begin{aligned} &= \sum_{i=1}^{6!} \int d\mathbf{q}'_1 d\mathbf{q}'_2 d\mathbf{q}'_3 d\mathbf{q}'_4 d\mathbf{q}'_5 d\mathbf{q}'_6 \\ &\quad \times \zeta^*(\mathbf{q}'_1, \mathbf{r}_1) \zeta^*(\mathbf{q}'_2, \mathbf{r}_2) \zeta^*(\mathbf{q}'_3, \mathbf{r}_3) \zeta^*(\mathbf{q}'_4, \mathbf{r}_4) \\ &\quad \times \zeta(\mathbf{q}'_{\sigma_i(3)}, \mathbf{r}_1) \zeta(\mathbf{q}'_{\sigma_i(4)}, \mathbf{r}_2) \zeta(\mathbf{q}'_{\sigma_i(5)}, \mathbf{r}_3) \zeta(\mathbf{q}'_{\sigma_i(6)}, \mathbf{r}_4) \\ &\quad \times \phi^*(\mathbf{q}'_{\sigma_i(1)}, \mathbf{q}'_{\sigma_i(2)}) \phi(\mathbf{q}'_5, \mathbf{q}'_6). \end{aligned} \quad (\text{A.30})$$

For ease of writing we now drop the primes.

$$\begin{aligned} &= \sum_{i=1}^{6!} \int d\mathbf{q}_1 d\mathbf{q}_2 d\mathbf{q}_3 d\mathbf{q}_4 d\mathbf{q}_5 d\mathbf{q}_6 \\ &\quad \times \zeta^*(\mathbf{q}_1, \mathbf{r}_1) \zeta^*(\mathbf{q}_2, \mathbf{r}_2) \zeta^*(\mathbf{q}_3, \mathbf{r}_3) \zeta^*(\mathbf{q}_4, \mathbf{r}_4) \phi(\mathbf{q}_5, \mathbf{q}_6) \\ &\quad \times \phi^*(\mathbf{q}_{\sigma_i(1)}, \mathbf{q}_{\sigma_i(2)}) \zeta(\mathbf{q}_{\sigma_i(3)}, \mathbf{r}_1) \zeta(\mathbf{q}_{\sigma_i(4)}, \mathbf{r}_2) \zeta(\mathbf{q}_{\sigma_i(5)}, \mathbf{r}_3) \zeta(\mathbf{q}_{\sigma_i(6)}, \mathbf{r}_4) \end{aligned} \quad (\text{A.31})$$

---

\*The initial indexing could have been done in a more concise way.

The number of possible permutations is extremely large (there are 720). These permutations can be identified as a representation of the symmetric group  $S_6$ . Since the bi-photon wave function is symmetric, this divides out all permutations where its indices are swapped since they are equivalent.

We will work out all of these cases.

### Case I: Identity

When the index belonging to the bi-photon wave function stays with its conjugate, for example where 1 and 2 get sent to 1 or 2 such that  $\zeta$  is still the complex conjugate while 5 and 6 get sent to 5 or 6 to not pick up the complex conjugation. If this is the case,

$$\begin{aligned} & \int dq_1 dq_2 dq_3 dq_4 dq_5 dq_6 \\ & \times \zeta^*(q_1, r_1) \zeta^*(q_2, r_2) \zeta^*(q_3, r_3) \zeta^*(q_4, r_4) \phi(q_5, q_6) \\ & \times \phi^*(q_1, q_2) \zeta(q_3, r_1) \zeta(q_4, r_2) \zeta(q_5, r_3) \zeta(q_6, r_4) \end{aligned} \quad (\text{A.32})$$

$$\begin{aligned} & = \int dq_1 dq_2 dq_3 dq_4 dq_5 dq_6 \\ & \times \zeta^*(q_1, r_1) \zeta^*(q_2, r_2) \phi^*(q_1, q_2) \\ & \times \zeta^*(q_3, r_3) \zeta(q_3, r_1) \zeta^*(q_4, r_4) \zeta(q_4, r_2) \\ & \times \zeta(q_5, r_3) \zeta(q_6, r_4) \phi(q_5, q_6). \end{aligned} \quad (\text{A.33})$$

$$= \Theta^{II*}(r_1, r_2) \Theta^{II}(r_3, r_4) \int dq_3 dq_4 \zeta^*(q_3, r_3) \zeta(q_3, r_1) \zeta^*(q_4, r_4) \zeta(q_4, r_2) \quad (\text{A.34})$$

$$= |\Theta^{II}(r_1, r_2)|^2 \Delta(r_1 - r_3) \Delta(r_2 - r_4). \quad (\text{A.35})$$

This makes sense; the single pairs can be detected in both detectors.

### Case II: Both Swapped

In this case we look at the cases where both indices are swapped:  $1, 2 \rightarrow 5, 6$  and  $5, 6 \rightarrow 1, 2$ . An example of this is worked out below where it is

used that the bi-photon wave function is real ( $\phi^* = \phi$ ).

$$\begin{aligned} & \int dq_1 dq_2 dq_3 dq_4 dq_5 dq_6 \\ & \times \zeta^*(q_1, r_1) \zeta^*(q_2, r_2) \zeta^*(q_3, r_3) \zeta^*(q_4, r_4) \phi(q_5, q_6) \\ & \times \phi^*(q_5, q_6) \zeta(q_3, r_1) \zeta(q_4, r_2) \zeta(q_1, r_3) \zeta(q_2, r_4) \end{aligned} \quad (\text{A.36})$$

$$\begin{aligned} & = \int dq_1 dq_2 dq_3 dq_4 dq_5 dq_6 \\ & \times \zeta^*(q_1, r_1) \zeta(q_1, r_3) \zeta^*(q_2, r_2) \zeta(q_2, r_4) \zeta^*(q_3, r_3) \zeta(q_3, r_1) \zeta^*(q_4, r_4) \zeta(q_4, r_2) \\ & \times \phi(q_5, q_6) \phi^*(q_5, q_6) \end{aligned} \quad (\text{A.37})$$

$$= \Gamma \Delta(r_1 - r_3)^2 \Delta(r_2 - r_4)^2 \quad (\text{A.38})$$

### Cases III: Single Swap

Another possibility is that one index is swapped to the ‘other side’, this means that  $1, 5 \rightarrow 1, 2$  and  $2, 6 \rightarrow 5, 6$ . For the permutation  $(1\ 5)$ :

$$\begin{aligned} & = \int dq_1 dq_2 dq_3 dq_4 dq_5 dq_6 \\ & \times \zeta^*(q_1, r_1) \zeta^*(q_2, r_2) \zeta^*(q_3, r_3) \zeta^*(q_4, r_4) \phi(q_5, q_6) \\ & \times \phi^*(q_5, q_2) \zeta(q_3, r_1) \zeta(q_4, r_2) \zeta(q_1, r_3) \zeta(q_6, r_4) \end{aligned} \quad (\text{A.39})$$

$$\begin{aligned} & = \int dq_1 dq_2 dq_3 dq_4 dq_5 dq_6 \\ & \times \zeta^*(q_1, r_1) \zeta(q_1, r_3) \zeta^*(q_3, r_3) \zeta(q_3, r_1) \zeta^*(q_4, r_4) \zeta(q_4, r_2) \\ & \times \zeta(q_6, r_4) \phi(q_5, q_6) \\ & \times \zeta^*(q_2, r_2) \phi^*(q_5, q_2) \end{aligned} \quad (\text{A.40})$$

$$= \int dq_5 \Theta^{2D}(r_4, q_5) \Theta^{2D*}(r_2, q_5) \Delta(r_1 - r_3)^2 \Delta(r_2 - r_4) \quad (\text{A.41})$$

### Discussion

Cases I, II and III show what happens when Eq. A.30 is worked out for different cases. The cases are non-zero, energy conservation is violated.

Permutations change the detector positions, the function should be symmetrical under these permutations because each order of detectors contributes just once. There are 720 possible permutations, all terms are one of the three cases above. To obtain the relative strength in intensity the contributions need to be counted. Perhaps group theory can help, the permutations are a representation of the symmetric group of size 6,  $S_6$ .

## A.2.2 Double Pair Wave Function

$$\begin{aligned}
& \langle \psi^{(2)} | \hat{E}^\dagger(\mathbf{r}_1) \hat{E}^\dagger(\mathbf{r}_2) \hat{E}^\dagger(\mathbf{r}_3) \hat{E}^\dagger(\mathbf{r}_4) \hat{E}(\mathbf{r}_4) \hat{E}(\mathbf{r}_3) \hat{E}(\mathbf{r}_2) \hat{E}(\mathbf{r}_1) | \psi^{(2)} \rangle \quad (\text{A.42}) \\
&= \langle vac | \int d\mathbf{q}_1 d\mathbf{q}_2 d\mathbf{q}_3 d\mathbf{q}_4 \phi^*(\mathbf{q}_1, \mathbf{q}_2) \phi^*(\mathbf{q}_3, \mathbf{q}_4) \hat{a}(\mathbf{q}_1) \hat{a}(\mathbf{q}_2) \hat{a}(\mathbf{q}_3) \hat{a}(\mathbf{q}_4) \\
&\times \int d\mathbf{q}'_1 d\mathbf{q}'_2 d\mathbf{q}'_3 d\mathbf{q}'_4 \zeta^*(\mathbf{q}'_1, \mathbf{r}_1) \zeta^*(\mathbf{q}'_2, \mathbf{r}_2) \zeta^*(\mathbf{q}'_3, \mathbf{r}_3) \zeta^*(\mathbf{q}'_4, \mathbf{r}_4) \hat{a}^\dagger(\mathbf{q}'_1) \hat{a}^\dagger(\mathbf{q}'_2) \hat{a}^\dagger(\mathbf{q}'_3) \hat{a}^\dagger(\mathbf{q}'_4) \\
&\times \int d\mathbf{q}_5 d\mathbf{q}_6 d\mathbf{q}_7 d\mathbf{q}_8 \zeta(\mathbf{q}_5, \mathbf{r}_1) \zeta(\mathbf{q}_6, \mathbf{r}_2) \zeta(\mathbf{q}_7, \mathbf{r}_3) \zeta(\mathbf{q}_8, \mathbf{r}_4) \hat{a}(\mathbf{q}_5) \hat{a}(\mathbf{q}_6) \hat{a}(\mathbf{q}_7) \hat{a}(\mathbf{q}_8) \\
&\times \int d\mathbf{q}'_5 d\mathbf{q}'_6 d\mathbf{q}'_7 d\mathbf{q}'_8 \phi(\mathbf{q}'_5, \mathbf{q}'_6) \phi(\mathbf{q}'_7, \mathbf{q}'_8) \hat{a}^\dagger(\mathbf{q}'_5) \hat{a}^\dagger(\mathbf{q}'_6) \hat{a}^\dagger(\mathbf{q}'_7) \hat{a}^\dagger(\mathbf{q}'_8) | vac \rangle \quad (\text{A.43})
\end{aligned}$$

The operators can be written as

$$\begin{aligned}
\hat{O} &= \hat{a}(\mathbf{q}_1) \hat{a}(\mathbf{q}_2) \hat{a}(\mathbf{q}_3) \hat{a}(\mathbf{q}_4) \hat{a}^\dagger(\mathbf{q}'_1) \hat{a}^\dagger(\mathbf{q}'_2) \hat{a}^\dagger(\mathbf{q}'_3) \hat{a}^\dagger(\mathbf{q}'_4) \\
&\times \hat{a}(\mathbf{q}_5) \hat{a}(\mathbf{q}_6) \hat{a}(\mathbf{q}_7) \hat{a}(\mathbf{q}_8) \hat{a}^\dagger(\mathbf{q}'_5) \hat{a}^\dagger(\mathbf{q}'_6) \hat{a}^\dagger(\mathbf{q}'_7) \hat{a}^\dagger(\mathbf{q}'_8) \quad (\text{A.44})
\end{aligned}$$

using Wick's theorem this can be written as

$$\hat{O} = \sum_{i=1}^{8!} \prod_{j=1}^8 \delta(\mathbf{q}_j - \mathbf{q}'_{\sigma_i(j)}) + \text{terms with operators}. \quad (\text{A.45})$$

Inserting this operator in the expression for the double photon wave function correlations yields

$$\begin{aligned}
& \sum_{i=1}^{8!} \int d\mathbf{q}_1 d\mathbf{q}_2 d\mathbf{q}_3 d\mathbf{q}_4 d\mathbf{q}_5 d\mathbf{q}_6 d\mathbf{q}_7 d\mathbf{q}_8 \\
&\times \phi^*(\mathbf{q}_1, \mathbf{q}_2) \phi^*(\mathbf{q}_3, \mathbf{q}_4) \zeta^*(\mathbf{q}_{\sigma_i(1)}, \mathbf{r}_1) \zeta^*(\mathbf{q}_{\sigma_i(2)}, \mathbf{r}_2) \zeta^*(\mathbf{q}_{\sigma_i(3)}, \mathbf{r}_3) \zeta^*(\mathbf{q}_{\sigma_i(4)}, \mathbf{r}_4) \\
&\times \phi(\mathbf{q}_{\sigma_i(5)}, \mathbf{q}_{\sigma_i(6)}) \phi(\mathbf{q}_{\sigma_i(7)}, \mathbf{q}_{\sigma_i(8)}) \zeta(\mathbf{q}_5, \mathbf{r}_1) \zeta(\mathbf{q}_6, \mathbf{r}_2) \zeta(\mathbf{q}_7, \mathbf{r}_3) \zeta(\mathbf{q}_8, \mathbf{r}_4). \quad (\text{A.46})
\end{aligned}$$

Again, three cases can be considered: 1. Identity, 2. Both Swapped, 3. Single Swap. The results gotten from the previous calculation are derived again for each case, along with magical other terms.

### Case I: Identity

In this case the permutation sends indices belonging to a bi-photon wave function to the same (any other or the original) wave function. An example

is worked out:

$$\begin{aligned} & \int dq_1 dq_2 dq_3 dq_4 dq_5 dq_6 dq_7 dq_8 \\ & \times \phi^*(q_1, q_2) \phi^*(q_3, q_4) \zeta^*(q_1, r_1) \zeta^*(q_2, r_2) \zeta^*(q_3, r_3) \zeta^*(q_4, r_4) \\ & \times \phi(q_5, q_6) \phi(q_7, q_8) \zeta(q_5, r_1) \zeta(q_6, r_2) \zeta(q_7, r_3) \zeta(q_8, r_4) \end{aligned} \quad (\text{A.47})$$

$$= \left| \Theta^{II}(r_1, r_2) \right|^2 \left| \Theta^{II}(r_3, r_4) \right|^2. \quad (\text{A.48})$$

The equality is obvious from the definition of  $\Theta^{II}$  compared to the definition of  $\zeta$ .

### Case II: Both Swapped

This swaps around the first four indices with the last four indices.

$$\begin{aligned} & \int dq_1 dq_2 dq_3 dq_4 dq_5 dq_6 dq_7 dq_8 \\ & \times \phi^*(q_1, q_2) \phi^*(q_3, q_4) \zeta^*(q_5, r_1) \zeta^*(q_6, r_2) \zeta^*(q_7, r_3) \zeta^*(q_8, r_4) \\ & \times \phi(q_1, q_2) \phi(q_3, q_4) \zeta(q_5, r_1) \zeta(q_6, r_2) \zeta(q_7, r_3) \zeta(q_8, r_4) \end{aligned} \quad (\text{A.49})$$

$$= \Gamma^2 \Delta(r_1 - r_1) \Delta(r_2 - r_2) \Delta(r_3 - r_3) \Delta(r_4 - r_4). \quad (\text{A.50})$$

Other permutations of the first four indices give different combinations in the  $\Delta$  function.  $\Delta(\mathbf{0}) = \frac{1}{4\pi^2}$ . This result raises some questions, since in this case a constant is added to the correlation function. This constant should be investigated.

### Case III: Single Swap

One wave function swapped

$$\begin{aligned} & \int dq_1 dq_2 dq_3 dq_4 dq_5 dq_6 dq_7 dq_8 \\ & \times \phi^*(q_1, q_2) \phi^*(q_3, q_4) \zeta^*(q_5, r_1) \zeta^*(q_6, r_2) \zeta^*(q_3, r_3) \zeta^*(q_4, r_4) \\ & \times \phi(q_1, q_2) \phi(q_7, q_8) \zeta(q_5, r_1) \zeta(q_6, r_2) \zeta(q_7, r_3) \zeta(q_8, r_4) \end{aligned} \quad (\text{A.51})$$

$$\begin{aligned} & = \int dq_1 dq_2 dq_3 dq_4 dq_5 dq_6 dq_7 dq_8 \\ & \times \phi^*(q_1, q_2) \phi(q_1, q_2) \\ & \times \phi^*(q_3, q_4) \phi(q_7, q_8) \zeta^*(q_3, r_3) \zeta^*(q_4, r_4) \zeta(q_7, r_3) \zeta(q_8, r_4) \\ & \times \zeta(q_5, r_1) \zeta^*(q_5, r_1) \zeta(q_6, r_2) \zeta^*(q_6, r_2) \end{aligned} \quad (\text{A.52})$$

$$= \Gamma \left| \Theta^{II}(r_3, r_4) \right|^2 \Delta(r_1 - r_1) \Delta(r_2 - r_2). \quad (\text{A.53})$$

Of course again with permutations of the positions.

**Case IV: Odd Swaps**

A single swap in a wave function

$$\begin{aligned} & \int dq_1 dq_2 dq_3 dq_4 dq_5 dq_6 dq_7 dq_8 \\ & \times \phi^*(q_1, q_2) \phi^*(q_3, q_4) \zeta^*(q_5, r_1) \zeta^*(q_2, r_2) \zeta^*(q_3, r_3) \zeta^*(q_4, r_4) \\ & \times \phi(q_1, q_6) \phi(q_7, q_8) \zeta(q_5, r_1) \zeta(q_6, r_2) \zeta(q_7, r_3) \zeta(q_8, r_4) \end{aligned} \quad (\text{A.54})$$

$$\begin{aligned} & \int dq_1 dq_2 dq_3 dq_4 dq_5 dq_6 dq_7 dq_8 \\ & \times \phi^*(q_1, q_2) \phi(q_1, q_6) \zeta^*(q_2, r_2) \zeta(q_6, r_2) \\ & \times \phi(q_7, q_8) \zeta(q_7, r_3) \zeta(q_8, r_4) \\ & \times \phi^*(q_3, q_4) \zeta^*(q_3, r_3) \zeta^*(q_4, r_4) \\ & \times \zeta(q_5, r_1) \zeta^*(q_5, r_1) \end{aligned} \quad (\text{A.55})$$

$$= \left| \Theta^H(r_3, r_4) \right|^2 \Delta(r_1 - r_1) \int dq_1 \left| \Theta^{2D}(q_1, r_2) \right|^2. \quad (\text{A.56})$$

**Case V: Even Swaps**

A single swap in two wave functions

$$\begin{aligned} & \int dq_1 dq_2 dq_3 dq_4 dq_5 dq_6 dq_7 dq_8 \\ & \times \phi^*(q_1, q_2) \phi^*(q_3, q_4) \zeta^*(q_5, r_1) \zeta^*(q_2, r_2) \zeta^*(q_7, r_3) \zeta^*(q_4, r_4) \\ & \times \phi(q_1, q_6) \phi(q_3, q_8) \zeta(q_5, r_1) \zeta(q_6, r_2) \zeta(q_7, r_3) \zeta(q_8, r_4) \end{aligned} \quad (\text{A.57})$$

$$\begin{aligned} & = \int dq_1 dq_2 dq_3 dq_4 dq_5 dq_6 dq_7 dq_8 \\ & \times \phi^*(q_1, q_2) \zeta^*(q_2, r_2) \phi^*(q_3, q_4) \zeta^*(q_4, r_4) \\ & \times \zeta^*(q_5, r_1) \zeta(q_5, r_1) \zeta^*(q_7, r_3) \zeta(q_7, r_3) \\ & \times \phi(q_1, q_6) \zeta(q_6, r_2) \phi(q_3, q_8) \zeta(q_8, r_4) \end{aligned} \quad (\text{A.58})$$

$$\begin{aligned} & = \int dq_1 dq_3 \Theta^{2D*}(q_1, r_2) \Theta^{2D*}(q_3, r_4) \Theta^{2D}(q_1, r_2) \Theta^{2D}(q_3, r_4) \\ & \times \Delta(r_1 - r_1) \Delta(r_3 - r_3) \end{aligned} \quad (\text{A.59})$$

$$= \Delta(r_1 - r_1) \Delta(r_3 - r_3) \int dq_1 dq_3 \left| \Theta^{2D}(q_1, r_2) \right|^2 \left| \Theta^{2D}(q_3, r_4) \right|^2. \quad (\text{A.60})$$

**Discussion**

It is difficult to know if these five cases contain all different classes of terms. How strong is each contribution? We need to count how much they contribute in some way, just as with the single pair terms.

# Appendix **B**

## Simulation

The equations to compute contain lots of integrals. This makes it computationally expensive to compute. Walborn's approximation for the spatial bi-photon wave function was used (Eq. 4.56) to reduce the computation time. The calculation was multi-threaded per pixel. The code will eventually be made available on GitHub\*.

The parameters for the simulation are listed in Table B.1, the settings for the simulation are listed in Table B.2.

---

\*<https://github.com/MioPoortvliet/four-photon-correlations>

Parameter	Value	description
width	2e4	Width of the peak of the bi photon wave function, the integrals are performed with a width of this number around the negative of the other momentum coordinate.
T	0.5	Transmittance of beamsplitter
R	0.5	Reflectivity of beamsplitter
B	1e-4	Interaction strength of PDC state, see Sabharwal's thesis for precise meaning
pump_wavelength	326e-9	Wavelength of pump beam
beam_waist	300e-6	Beam waist of pump beam (assuming focus in crystal)
beam_waist_slm	900e-6	Beam waist of the projected onto modes (in this case the SLMs)
n_p	1.7468	Refractive index at pump wavelength
n_s	1.8103	Refractive index at down-converted wavelength
poling_period	3.875e-6	Poling period of crystal
crystal_length	5e-2	Length of crystal in the direction of beam travel
lp	0	$l_p$ , OAM of pump beam
pp	0	$p_p$ , $p$ of pump beam

**Table B.1:** Parameters used throughout all calculations.

Setting	Used Value	Description
L_transverse	$[1.1e - 3, 1.1e - 3]$	Dimensions of plane to plot
z	$250e - 3$	z-distance the calculation is done at
resolution	50	Width and height of the plane in pixels
threads	12	Threads to use during the calculation
debug	1	Debug verbosity, higher is more verbose
epsrel	1.5e-2	Relative error allowed by integration package (scipy.integrate.nquad)
only_diagonals	false	Only calculate points on diagonals?
export_path		Path to export plots to
calc_what	"all"	Calculates both G2 and Gind
thin_crystal_limit	false	Use thin crystal limit? ( $\phi(q_1, q_2) = 1$ )

**Table B.2:** Settings used to calculate the simulation of G2.

## Acknowledgments

The first day I entered Leiden University I already looked forward to my bachelor's research project. I would finally be allowed to do a serious project and I would get to experiment in a lab. For this reason, the first month of my bachelor project was amazing. Then the 2020 pandemic started and the university closed. The largest part of my bachelor's project was spent at home, outside of the lab. In no way was this disappointing however, the amazing people in the quantum optics group ensured I had a great time.

First, I want to thank Dr. Wolfgang Löffler for his excellent guidance and allowing me to complete my bachelor's research project in his group. Wolfgang has provided guidance to me beyond what I expected. This includes regular group meetings and patient one-on-one talks to pick my brain and help me progress in this project. Wolfgang spent a lot of time in the lab when I was not allowed to. He set up remote measurement capabilities, aligned the optics and dealt with frustrating problems. Thank you for your patience and effort.

I would like to also thank the second corrector Prof. Dr. Serge Fehr. Thank you for taking the time and effort to read through this thesis, I hope you have enjoyed it.

Further, I would like to thank the people in Wolfgang's research group. During group meetings insightful discussions were had. Outside of group meetings we also had fun: office jenga, lunch table toys, tesla coils, the uncomfortable hammock and that guitar missing most of its strings. I never had a boring time and look back on my interactions with all of you with fond memories. Thank you, Matteo, Petr, Kirsten, Giel, Jonathan, David, Oliver, Daniël and (during the last few weeks) Florine.

I am grateful to my dear friend Jonah Post who was kind enough to provide feedback on this thesis. Your comments have improved the readability and structure of this thesis by a lot. I value your input; I also value our friendship and the discussions (sometimes about physics) we have had during the bachelor. Thank you, Jonah.

I would like to thank my love Roos Vreman for literally and figuratively being beside me during the quarantine. Wolfgang and his group have seen and heard her during group meetings, she walked around in the background or had her own meetings. When the camera was off she would offer me lots of support and motivation. I am glad she was there, without Roos I would not have had as much discipline or structure in my life during quarantine to put the necessary time and effort into my bachelor's project.

Finally I want to express my thanks to the many scientist whose work is the basis of this thesis.

I wish I had more time to do the next step in this project, do another measurement and read more theory. Still, I am proud of how this project turned out.

To the people picking up where I left off: my hope is that this thesis provides you with a basis to start from. It took me the larger part of the time available for the bachelor thesis to understand PDC. I have done all I can to write down the theory in a clear and structured way, hopefully bridging the gap from undergraduate physics to specialized quantum optics literature. Go make beautiful things happen, though difficult I found the material very fulfilling. Best of luck!



# Bibliography

- [1] A. Einstein, B. Podolsky, and N. Rosen, *Can Quantum-Mechanical Description of Physical Reality Be Considered Complete?*, *Physical Review* **47**, 777 (1935).
- [2] T. Holz, H. Kampermann, and D. Bruss, *A Genuine Multipartite Bell Inequality for Device-independent Conference Key Agreement*, arXiv:1910.11360 [quant-ph] (2019), arXiv: 1910.11360.
- [3] Mark Hillery, Vladimír Bužek, and André Berthiaume, *Quantum Secret Sharing*, **59** (1999).
- [4] M. de Oliveira, I. Nape, J. Pinnell, N. TabeBordbar, and A. Forbes, *Experimental quantum secret sharing with spin-orbit structured photons*, arXiv:1909.01147 [physics, physics:quant-ph] (2019), arXiv: 1909.01147.
- [5] I.-C. Yu, F.-L. Lin, and C.-Y. Huang, *Quantum secret sharing with multilevel mutually (un)biased bases*, *Physical Review A* **78**, 012344 (2008).
- [6] J. P. Torres, Y. Deyanova, L. Torner, and G. Molina-Terriza, *Preparation of engineered two-photon entangled states for multidimensional quantum information*, *Physical Review A* **67**, 052313 (2003).
- [7] J. P. Torres, A. Alexandrescu, and L. Torner, *Quantum spiral bandwidth of entangled two-photon states*, *Physical Review A* **68**, 050301 (2003).
- [8] N. Quesada and J. E. Sipe, *Why you should not use the electric field to quantize in nonlinear optics*, *Optics Letters* **42**, 3443 (2017).
- [9] J. Schneeloch, S. H. Knarr, D. F. Bogorin, M. L. Levangie, C. C. Tison, R. Frank, G. A. Howland, M. L. Fanto, and P. M. Alsing, *Introduction*

- to the absolute brightness and number statistics in spontaneous parametric down-conversion*, *Journal of Optics* **21**, 043501 (2019).
- [10] S. Trajtenberg-Mills, A. Karnieli, N. Voloch-Bloch, E. Megidish, H. S. Eisenberg, and A. Arie, *Simulating Correlations of Structured Spontaneously Down-Converted Photon Pairs*, *Laser & Photonics Reviews* **14**, 1900321 (2020).
- [11] W. Wieczorek, C. Schmid, N. Kiesel, R. Pohlner, O. Gühne, and H. Weinfurter, *Experimental observation of an entire family of four-photon entangled states*, *Physical Review Letters* **101**, 010503 (2008), arXiv: 0806.1882.
- [12] S. Franke-Arnold, S. M. Barnett, M. J. Padgett, and L. Allen, *Two-photon entanglement of orbital angular momentum states*, *Physical Review A* **65**, 033823 (2002).
- [13] A. Mair, A. Vaziri, G. Weihs, and A. Zeilinger, *Entanglement of the orbital angular momentum states of photons*, **412**, 4 (2001).
- [14] X.-F. Ren, G.-P. Guo, B. Yu, J. Li, and G.-C. Guo, *The orbital angular momentum of down-converted photons*, *Journal of Optics B: Quantum and Semiclassical Optics* **6**, 243 (2004).
- [15] S. Feng and P. Kumar, *Spatial Symmetry and Conservation of Orbital Angular Momentum in Spontaneous Parametric Down-Conversion*, *Physical Review Letters* **101**, 163602 (2008), Publisher: American Physical Society.
- [16] M. Malik, M. Erhard, M. Huber, M. Krenn, R. Fickler, and A. Zeilinger, *Multi-photon entanglement in high dimensions*, *Nature Photonics* **10**, 248 (2016).
- [17] B. C. Hiesmayr, M. J. A. de Dood, and W. Löffler, *Observation of Four-Photon Orbital Angular Momentum Entanglement*, *Physical Review Letters* **116** (2016).
- [18] F. L. Pedrotti and L. S. Pedrotti, *Introduction to Optics*, Prentice-Hall, New Jersey, 2 edition, 1993.
- [19] A. Lepidis, *On Quadripartite Entanglement in High-Dimensional Hilbert Space*, PhD thesis, Leiden University, Leiden, The Netherlands, 2019.
- [20] C. Bender, *Towards 4-photon OAM entanglement experiments*, PhD thesis, Leiden University, Leiden, The Netherlands, 2019.

- 
- [21] F. Pampaloni and J. Enderlein, *Gaussian, Hermite-Gaussian, and Laguerre-Gaussian beams: A primer*, page 29.
- [22] L. Allen, M. W. Beijersbergen, R. J. C. Spreeuw, and J. P. Woerdman, *Orbital angular momentum of light and the transformation of Laguerre-Gaussian laser modes*, *Physical Review A* **45**, 8185 (1992).
- [23] F. Zernike and J. E. Midwinter, *Applied Nonlinear Optics*, Dover Publications, Mineola, 2006.
- [24] A. Yariv, *Quantum Electronics*, John Wiley & Sons, United States of America, 2 edition, 1975.
- [25] H. Pires, *Spatial coherence and entanglement of light*, s.n., S.l., 2011, OCLC: 752895957.
- [26] W. H. Peeters, *Two-photon Interference*, PhD thesis, Leiden University, Leiden, The Netherlands, 2010.
- [27] B.-J. Pors, *Entangling light in high dimensions*, s.n., S.l., 2011, OCLC: 700926526.
- [28] M. V. Fedorov, M. A. Efremov, P. A. Volkov, E. V. Moreva, S. S. Straupe, and S. P. Kulik, *Spontaneous parametric down-conversion: Anisotropic and anomalously strong narrowing of biphoton momentum correlation distributions*, *Physical Review A* **77** (2008).
- [29] H. Di Lorenzo Pires, F. M. G. J. Coppens, and M. P. van Exter, *Type-I spontaneous parametric down-conversion with a strongly focused pump*, *Physical Review A* **83**, 033837 (2011).
- [30] R. Graham, *General Correlation Identity for Parametric Processes*, *Physical Review Letters* **52**, 117 (1984).
- [31] P. A. Franken and J. F. Ward, *Optical Harmonics and Nonlinear Phenomena*, *Reviews of Modern Physics* **35**, 23 (1963).
- [32] J.-C. Lee and Y.-H. Kim, *Spatial and spectral properties of entangled photons from spontaneous parametric down-conversion with a focused pump*, *Optics Communications* **366**, 442 (2016).
- [33] D. A. Kleinman, *Nonlinear Dielectric Polarization in Optical Media*, *Physical Review* **126**, 1977 (1962).
-

- 
- [34] J. Schneeloch and J. C. Howell, *Introduction to the Transverse Spatial Correlations in Spontaneous Parametric Down-Conversion through the Biphoton Birth Zone*, *Journal of Optics* **18**, 053501 (2016), arXiv: 1502.06996.
- [35] C. Couteau, *Spontaneous parametric down-conversion*.
- [36] C. C. Gerry and P. L. Knight, *Introductory Quantum Optics*, Cambridge University Press, Cambridge, UK, ebook edition, 2005.
- [37] L. Shiqun and W. Ligan, *Degenerate Parametric Down Conversion of Squeezed Light*, *Chinese Physics Letters* **8**, 222 (1991).
- [38] R. W. Boyd, *Nonlinear Optics*, Academic Press, 3 edition.
- [39] C. K. Hong and L. Mandel, *Theory of parametric frequency down conversion of light*, *Physical Review A* **31**, 2409 (1985).
- [40] S. Sabharwal, *Spatial Bunching of Entangled Four Photons*, page 53.
- [41] R. Paschotta, *Birefringent Phase Matching*, Library Catalog: [www.rp-photonics.com](http://www.rp-photonics.com).
- [42] R. Paschotta, *Quasi-phase Matching*, Library Catalog: [www.rp-photonics.com](http://www.rp-photonics.com).
- [43] R. Paschotta, *Periodic Poling*, Library Catalog: [www.rp-photonics.com](http://www.rp-photonics.com).
- [44] J. A. Armstrong, N. Bloembergen, J. Ducuing, and P. S. Pershan, *Interactions between Light Waves in a Nonlinear Dielectric*, *Physical Review* **127**, 1918 (1962).
- [45] Thorlabs, *Periodically Poled Lithium Niobate (PPLN) - Tutorial*, Self Published .
- [46] A. Arie, N. Habshoosh, and A. Bahabad, *Quasi phase matching in two-dimensional nonlinear photonic crystals*, *Optical and Quantum Electronics* **39**, 361 (2007).
- [47] D. N. Klyshko, *COMBINED EPR AND TWO-SLIT EXPERIMENTS: INTERFERENCE OF ADVANCED WAVES*, *PHYSICS LETTERS A* **132**, 6 (1988).
- [48] A. V. Belinskii and D. N. Klyshko, *Two-photon optics: diffraction, holography, and transformation of two-dimensional signals*, page 487 (1994).

- [49] M. F. Z. Arruda, W. C. Soares, S. P. Walborn, D. S. Tasca, A. Kanaan, R. Medeiros de Araújo, and P. H. Souto Ribeiro, *Klyshko's advanced-wave picture in stimulated parametric down-conversion with a spatially structured pump beam*, *Physical Review A* **98**, 023850 (2018).
- [50] Y. Zhang, M. McLaren, F. S. Roux, and A. Forbes, *Simulating quantum state engineering in spontaneous parametric down-conversion using classical light*, *Optics Express* **22**, 17039 (2014).
- [51] L. G. Helt, M. Liscidini, and J. E. Sipe, *How does it scale? Comparing quantum and classical nonlinear optical processes in integrated devices*, *Journal of the Optical Society of America B* **29**, 2199 (2012).
- [52] R. Paschotta, *Sech<sup>2</sup>-shaped Pulses*, Library Catalog: [www.rp-photonics.com](http://www.rp-photonics.com).
- [53] R. Paschotta, *Gaussian Pulses*, Library Catalog: [www.rp-photonics.com](http://www.rp-photonics.com).
- [54] S. P. Walborn, A. N. de Oliveira, R. S. Thebaldi, and C. H. Monken, *Entanglement and conservation of orbital angular momentum in spontaneous parametric down-conversion*, *Physical Review A* **69**, 023811 (2004).
- [55] C. K. Law and J. H. Eberly, *Analysis and Interpretation of High Transverse Entanglement in Optical Parametric Down Conversion*, *Physical Review Letters* **92** (2004).
- [56] M. Fedorov, *Schmidt decomposition for non-collinear biphoton angular wave functions*, arXiv:1411.2144 [quant-ph] (2014), arXiv: 1411.2144.
- [57] L. Lamata and J. Leon, *Dealing with entanglement of continuous variables: Schmidt decomposition with discrete sets of orthogonal functions*, *Journal of Optics B: Quantum and Semiclassical Optics* **7**, 224 (2005), arXiv: quant-ph/0410167.
- [58] H. D. Riedmatten, V. Scarani, I. Marcikic, A. Acín, W. Tittel, H. Zbinden, and N. Gisin, *Two independent photon pairs versus four-photon entangled states in parametric down conversion*, *Journal of Modern Optics* **51**, 1637 (2004).
- [59] S. Ç. Yorulmaz, *Beyond Photon Pairs*, PhD thesis, Leiden University, 2014.
- [60] D. Walls and G. J. Millburn, *Quantum Optics*.

- [61] A. Y. Bekshaev and A. I. Karamoch, *Structure of optical vortices produced by holographic gratings with "fork" geometry: Kummer beams*, page 12 (2007).